Observations and modeling of alongshore variation in dune erosion

Florine Gongriep (3286061)

MSc Thesis
MSc Earth Surface and Water

Supervisors:
Prof. dr. B. G. Ruessink
MSc Renske de Winter

Coastal Research Group
Department of Physical Geography
Faculty of Geosciences
Utrecht University
The Netherlands
21-10-2013

Observations and modelling of alongshore variation in dune erosion

Florine Gongriep (3286061)

MSc Thesis – 21-10-2013

Supervisors:
Prof. dr. B. G. Ruessink (Utrecht University)
MSc Renske de Winter (Utrecht University)

Department of Physical Geography
Faculty of Geosciences
Utrecht University
The Netherlands

Contents

List of figures and tables

(d) the eroded volume *V1* between the top of the dune face to the pre-erosion event dune foot, for the measured topography (black), the topography with a uniform bathymetry (blue) and the topography with a uniform dune row (green).
Figure 24 (a) The initial topography with the uniform bathymetry. The pink dots indicate the locations where the Hm0,ss and Hm0,inf were calculated. These were located at three alongshore shore transects at x = -8.9 m, x = 78.1 m and x = 325.0 m and one cross-shore transect at y = - 216.5 m. (b), (c), (d) show the calculated Hm0,ss (blue) and Hm0,inf (cyan) along the alongshore transects and (e) along the cross-shore together with the topography profile (green) and the mean surge level (pink). (f) shows the predicted topographical difference map, also with the output locations.
Figure 25 (a) The observed initial topography. The pink dots indicate the locations where the Hm0,ss and Hm0,inf were calculated. These were located at three alongshore shore transects at x = -8.9 m, x = 78.1 m and x = 325.0 m and one cross-shore transect at y = - 216.5 m. (b), (c), (d) show the calculated Hm0,ss (blue) and Hm0,inf (cyan) along the alongshore transects and (e) along the cross-shore together with the topography profile (green) and the mean surge level (pink). (f) shows the predicted topographical difference map, also with the output locations.

Table 1. Mean wave conditions per period, which are used to create the wave conditions at the offshore boundary.
Table 2. The quantified errors for the results of the validation performed in 2D mode.
Table 3. The quantified errors for the results of the validation performed in 2D mode.

Abstract

The dunes form the primary protection against the sea in the Netherlands, but they can only withstand the sea during storms when they are high and wide enough. It is therefore of vital importance for the Dutch population that the safety of the dunes is assessed regularly. At present the DUROS+ model is used for this assessment, which gives good results for approximately straight and uniform coasts. However, a process-based model could give better results for more complex areas. The process-based model Xbeach has shown potential to predict dune erosion under an extensive amount of controlled laboratory experiments, but only few validations have been performed based on field data. Therefore we performed a hydrodynamic and morphodynamic validation, based on a field data set that was obtained near Egmond aan Zee. The hydrodynamic validation showed that XBeach predicts the Hm0 infragravity wave height reasonably well, with a ε_{rms} of 0.086 and a r^2 of 0.92, but that the short wave height is overestimated, with an ε_{rms} of 0.043 and a r^2 of 0.29. The morphologic validation showed that the dunefoot retreat predicted by XBeach was 37% higher than the average observed dunefoot retreat and the eroded volume was over predicted by 76 %, but XBeach was capable to reproduce the alongshore trends in the observed dune erosion reasonably well. Furthermore, XBeach predicted alongshore variation in the eroded volume for both a topography with a uniform bathymetry and a topography with a uniform dune topography, which proved that both alongshore variation in the dune and beach topography and alongshore variation in the bathymetry lead to alongshore variation in the eroded volume.

1. Introduction

In the Netherlands, the primary protection against the sea is formed by the long stretch of dunes along the North Sea coast (Vellinga, 1986; van Baak, 2002 ; van Thiel de Vries, 2008; Hoonhout and den Heijer, 2010). This natural buffer is primarily built by aeolian transport. During storms when the sea level rises considerably above normal high water level and powerful waves reach the dunes, the dunes erode. To withstand the sea for the duration of the storm or a sequence of storm events, the dunes must be high and wide enough (Vellinga, 1986; Carter, 1989; Splinter and Palmsten, 2012). This is of vital importance for the Dutch population because approximately half of the Netherlands lies below mean sea level and the narrow stretch of sand beaches and dunes forms the principal protection against the sea. Flooding of the lower lying hinterland due to overwash or inundation may have devastation consequences, because this area is highly populated and of high economic value for the Netherlands. A flood might even disrupt a large part of the country and full recovery may take years (Vellinga, 1986).

This was illustrated by the dramatic event in 1953, when the sea level became exceptionally high during a storm and large areas flooded in the SouthWest of the Netherlands. Many lives and properties were lost to the water. This increased the awareness of the dangers of living below sea level. Everybody agreed that such a disaster should never happen again. The Delta Committee was created to design coastal protection measures and to make and implementation plans. This committee devised a new Law on Water Defences which was approved in 1957 (De Haan and Haagsma, 1984). One of the requirements of this law was that models would be developed in order to enable the government to perform dune strength assessments. These models should predict where the dunes would become too vulnerable so that a future breach would be avoided (Hoonhout and den Heijer, 2010). Many models have been developed since.

Assessment of the dunes is still a priority, not only to avoid large scale flooding, but also to avoid coastal retreat locally when it endangers highly populated and cultivated coastal areas. Therefore the coastline is kept in a fixed position. Unfortunately this also causes dune erosion, because natural processes that lead to accretion of the dunes are disrupted due to the loss of dynamics. If net erosion takes place expensive reinforcement works, like nourishments, become necessary to avoid coastal retreat. The Dutch government assesses the strength of the dunes against normative storm conditions every six years. There is an ongoing debate on the required safety level against flooding (Brandenburg, 2010). Currently the law prescribes that a row of dunes should be able to withstand a probability 1:10,000 storm event at the most valuable parts of the coast and slightly lower in other parts. (van Baak, 2002; WL | Delft hydraulics, 2006; den Hijer, 2008; van Thiel de Vries, 2009).

At present the DUROS+ model is used for the safety assessments in the Netherlands, which has been developed by Van Gent *et al.* (2008). It is based on the DUROS model build by Vellinga (1986, 1982), who used empirical relations for this model which he derived from a large series of laboratory experiments. DUROS+ is an empirical model which is based on the assumption that the beach profile always tends to be in equilibrium with the external conditions, like the waves and the surge level. Many of the physical parameters are directly linked to post-storm profiles and therefore not quantified individually (Brandenburg, 2010). The advantage of DUROS+ is that it generates results quickly, but in strict sense they are only valid for approximately straight and uniform coasts, which can be assumed to be infinitely long. However, often those prerequisites are not met along the Dutch coast, because it contains curvatures and non-uniform areas with for example inlets, large shoals or an alongshore gradient caused by other features (Vellinga, 1986; van Thiel de Vries *et al*, 2008; Hoonhout and den Heijer, 2010). Empirical models are therefore not capable of predicting the safety level accurately everywhere along the Dutch coast. (Vellinga, 1986; Steetzel, 1993; Nishi and Kraus, 1996; Roelvink *et al.,* 2010; den Heijer *et al.*, 2011). It would require many more experiments and possibly new research facilities to find the empirical relationships needed to include more complex areas into empirical models (van Thiel de Vries, 2011).

Steelzel (1993) proposed to develop more generic dune erosion models as a solution to this problem. Several generic time-depended models have been developed over the last decades, most of which are based on calculations of the cross-shore transport of sediment (Splinter and Palmsten, 2012). Examples of process-based models are Durosta, Crosmor and XBeach developed by Steelzel (1993), van Rijn (2008) and Roelvink *et al.* (2009), respectively. The Dutch governmental organization 'Rijkswaterstaat' expressed a desire to work with such a model (van Thiel de Vries, 2009; Roelvink *et al*., 2010).

Xbeach has been designed to make more advanced safety predictions for complex areas and to enable scientists to understand better the processes that are observed along beaches. It can be used for complex areas, because the model predictions are based on the physical processes that drive dune erosion in contrast to the empirical models. XBeach combines those processes to calculate the evolution of the cross-shore profile. This also enables calculating alongshore processes and the resulting alongshore variability in dune erosion. Furthermore, XBeach enables scientists to explore dune erosion under new external conditions, which is interesting with regard to climate change research. It is possible that the Dutch dunes cannot meet the safety standard anymore in the future as a result of sea level rise (Hoonhout and den Heijer, 2010).

Xbeach has shown potential to predict dune erosion under an extensive amount of controlled laboratory experiments, but only few validations have been performed using field data (Roelvink *et al*., 2009; McCall *et al*., 2010; Splinter and Palmsten, 2012). Field validations are important because relations that are experimentally found in a laboratory must always be scaled up to field scale, which

increases uncertainties significantly (Brandenburg, 2010; Van Rijn, 2011). In addition, field validations are needed to verify model predictions on alongshore variation, because the current laboratory facilities are not wide enough to include alongshore processes (van Thiel de Vries, 2011).

The objective of this study is to perform a quantitative hydrodynamic and morphologic field-scale validation of Xbeach, based on a field data set that was obtained near Egmond aan Zee. The hydrodynamic forcing of XBeach will be validated by comparing the predicted to the observed infragravity and short wave height transformation in the intertidal zone for different offshore wave conditions. The morphologic validation will be performed by comparing observed and predicted dune erosion in response to a northwesterly storm observed from 3 until 6 January 2012. Large differences in dune erosion were observed alongshore, from a minor 1 m high cliff up to slumping of the entire dune face. This makes it possible to explore the capability of Xbeach to predict alongshore variation in dune erosion.

The main research questions are:

- How do Xbeach simulations compare to field observations of cross-shore wave transformation in the intertidal zone during severe storms?
- How do XBeach simulations compare to field observations of dune erosion and alongshore variation thereof?
- What causes the observed and predicted alongshore variation in the dune erosion pattern?

The outline of this thesis is as follows. First more background will be provided on dune erosion observations and on Xbeach (chapter 2). Then, in chapter 3, the hydrodynamic calibration and validation of XBeach will be presented. In chapter 4, the morphologic data set will be described, followed by a description of the observed dune erosion and a comparison to the model predictions. Furthermore we will explore the causes of alongshore variation in the dune erosion. Finally the results are discussed in chapter 5 and the conclusions are given in chapter 6.

2. Literature review

2.1 Dune erosion observations

2.1.1 Introduction

In the Netherlands, the primary protection against the sea is formed by a long stretch of sandy dunes. They form a natural buffer of loose, dispersible sediments which protects the hinterland. Compared to other types of coasts they evolve relatively rapidly in time. Dunes continuously change shape in response to the external conditions, like the wind and the waves. During severe storm conditions dune erosion rates can become very high, sometimes up to several meters per hour. Still, when the dune row is high and wide enough, it can withstand large seas. The reason for this is that severe erosion usually only takes place during short time periods; often only during high tides combined with storms. When conditions become more tranquil after the storm passed the dunes start to accrete again (Vellinga, 1986; Carter, 1989).

2.1.2 Observed dune erosion processes

When a low-pressure field passes over the North Sea in southeasterly direction strong winds are generated that initially come from the southwest. When the depression passes they shift to the northwest. The sea level may rise considerably above normal high water level due to the shear stresses that the wind exerts on the surface and because the air pressure that is pressing down on the water is lower in the depression. In combination with the high tides this may lead to a sea level rise of 5-8 meters above average in extreme cases (Vellinga, 1986; Carter, 1989; Brandenburg, 2010). Powerful storm driven waves can already reach the front of the dunes generally when the surge level is 1 to 2 m above high tide level.

The dune foot is relatively steep; therefore the wave energy is dissipated over a very short distance, creating a turbulent environment. The sediment that is suspended due to the turbulence settles further seaward where the turbulence is less. When the first series of waves reach the dune front, the dune foot becomes saturated, undercutting takes place and sediment slouches onto the beach. This process continues till the undercutting erodes the dune foot to such an extent that the dune front becomes unstable (Vellinga 1986; Nishi and Kraus, 1996; Brandenburg, 2010)

This may have various consequences. First of all sediment might slide down towards the beach zone known as avalanching (Carter 1989; Nishi and Kraus, 1996). However, when the dune face gets very steep, it is more likely that layers separate; a vertical crack develops parallel to the slope due to a sequence of wave impacts and the layer, with a typical thickness of 30 to 50 centimetres, gets separated from the main body. This layer collapses or even overturns when it is tilted forward (Nishi and Kraus, 1996). These failures are often observed when the slope is poorly vegetated. If the dune face is better vegetated, the waves can cut deeper into the dune base before the overlying layer collapses. It collapses when the notch gets so deep that the upward forces in the overhanging layer become smaller than the downward gravity force on the layer. Usually the sediment comes down in pseudo-shear plane slides when it fails (Vellinga 1986; Carter 1989; Nishi *et al*, 1996). When a slope is very well vegetated it might take up to a few days till it collapses. Typically this results in retrogressive slumping, often in the form of a shallow rotational slide across the entire dune face. The

vegetation and root-mat form a strong cover along the shore that only slowly deteriorates. This cover can withstand several months of storm before exposing the bare dune face (Carter, 1989).

The differences in failure can be related to the vegetation density, the root mat that it develops and the compaction of the sediment due to natural settling and wetting of the sediment. The higher the vegetation density, cohesiveness and compaction of the sediment, the steeper the dune faces can be after erosion. The bulk density, the slope re-sedimentation and moisture- and salt content determine the shear stress in the dune face (Carter, 1989; Nishi and Kraus, 1996).

The sediment that is deposited on the beach forms a pile of sediment in front of the dune foot. It protects the dune and therefore slows down the erosion process for all the failure types to a greater or lesser extend. After some 50 to 100 waves the pile of sand is cleared away by wave action and the waves will impact the dune front again. It is sometimes assumed that the erosion of the dunes is fully controlled by the sediment transport capacity of the breaking waves and that the resistant forces are relatively unimportant to the rate and quantity of dune erosion (Vellinga, 1982; Vellinga, 1986; Brandenburg, 2010).

Most of the sediment that is introduced into the swash zone is transported to the inner surf zone. The swash action provides a major mechanism for cross-shore sediment exchange between the sub-aerial and sub-aqueous zones of the beach, because the sediment concentrations are very high, as a result of the high dynamics and flow velocities forced by the waves. Also, the infragravity wave energy tends to increase shoreward and is therefore predominant in the swash zone during high-energy conditions. The offshore-directed swash motion is called the backswash. This transports the sediment into the inner surf zone (Vellinga, 1986; Butt and Russel, 1999; Masselink et al, 2005; van Thiel de Vries, 2009; Roelvink *et al*, 2010).

In the surf zone processes forced by the breaking waves take over. These processes cannot exist in the swash zone, because the beach has to be submerged hundred percent of the time (Vellinga, 1986; Butt and Russel, 1999; Roelvink *et al*,. 2010). When waves enter the surf zone and break, it results in the transfer of momentum and the dissipation of part of their energy. Consequently their height decreases but their mass is conserved and therefore water piles up against the shoreline which leads to an increased water level close to the shore. This wave set-up creates an offshore-directed hydrostatic pressure gradient which results in a mean cross-shore back flow called ‘the undertow’ or in three-dimensional rip cell currents (van Thiel de Vries, 2008; Davidson-Arnott, 2010). During severe storms the undertow is the most prevalent current type, because the three-dimensionality in the morphology is erased (Vellinga, 1986; Russell and Huntley, 1999; Davidson-Arnott, 2010).

Most of the eroded sediment that is transported in the cross-shore direction settles seaward where the undertow and the turbulence caused by the breaking waves becomes less (van Thiel de Vries, 2011). This changes the shape of the cross-shore profile, but the total sediment content of the profile is conserved if there is no alongshore transport. It has been observed that a more elevated and evenly sloping beach profile develops (van Gent *et al.* 2008). Figure 1 shows the initial pre-storm beach profile and a schematized eroded profile afterwards. As a consequence of the gentler beach slope, wave energy is dissipated over a larger distance and the offshore transport capacity and thus dune erosion rate will decrease with time (Vellinga, 1986). If the storm would continue long enough, eventually a new profile with a constant shape would be reached that is in equilibrium with the external conditions. However, this hardly ever happens during a single storm surge, because the storm will die out before this new equilibrium state can be reached (Vellinga, 1986; Carter, 1989; McCall, 2008; van Thiel de Vries, 2009).

An exception to the rule is the case where the eroded sediment is transported away by an alongshore current and no sediment is supplied from upstream. The beach stays steep and the dunes

will keep feeding the beach. This often leads to long-term coastal retreat (Vellinga, 1986; Carter 1989; van Thiel de Vries, 2011).

After the storm has passed, the cross-shore profile will start to change again to a shape that corresponds to more tranquil conditions. Field observations indicate that the deposited sediment that lies not to far seaward will return to the beach due to the wave action. Also, the dunes will start to recover when Aeolian transport transports dry beach sediment to the dunes and the vegetation retains it there. In the field equilibrium will be reached hardly ever because the external conditions are too unsteady.

The length of the period between one erosion event and the next is important as it determines the state of recovery of the dunes and this controls the rate of erosion during the next storm. Full recovery might take several month or longer. Within a few years the dunes might start to advance seawards again (Vellinga, 1986; Carter 1989; van de Graaff, 2002; Davidson-Arnott, 2010).

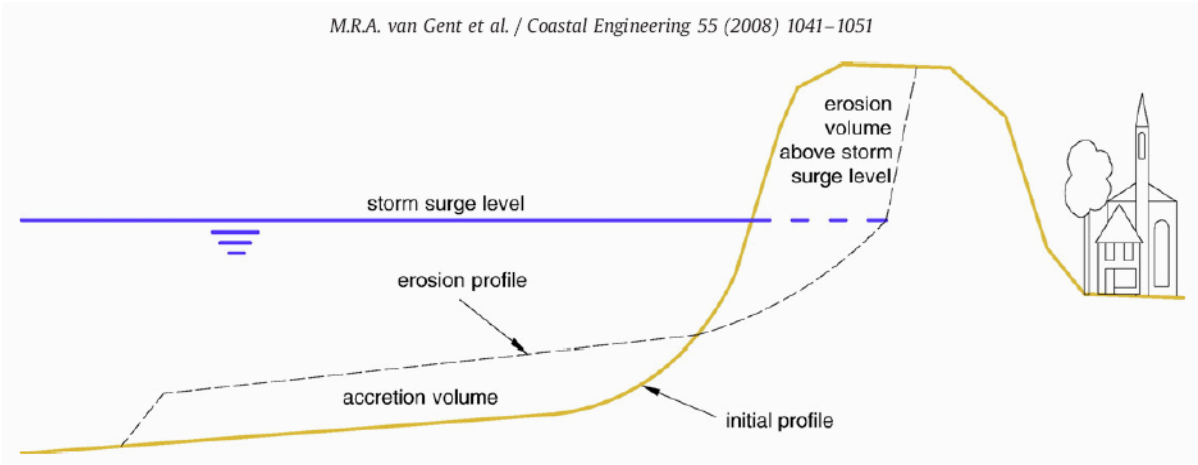

Figure. 1. Initial cross-shore profile and erosion profile after an extreme storm event (Van Gent *et al.* 2008).

2.1.3 Infragravity waves

This study focuses on flat, dissipative beaches instead of reflective beaches, where the shallow water area is relatively long and the incident waves break in a wide surf-zone. At these beaches the incident short period- or short waves, like sea and swell, are often embedded within long-period motions, called long waves or infragravity waves. Infragravity wave frequencies grow when the wind picks up and the wave height of the sea swell increases, because the wave energy of short incident waves is transferred to the infragravity waves. (Tucker, 1954; Corps of engineers, 1989; Elgar et al., 1992; Butt and Russell, 1999; Sheremet, et al., 2002; McCall, 2008). Field measurements have shown that infragravity waves become dominant during high-energy dissipative conditions, which are characteristic for the Dutch coast during severe storms (Corps of engineers, 1989; Butt and Russell, 1999; McCall, 2008; Van Gent *et al.* 2008). Furthermore, observations showed that infragravity waves might be responsible for 80 to 100% of the surf- and swash zone elevation on dissipative beaches (Corps of engineers, 1989). This leads to a higher sediment suspension, which increases the offshore transport. The rate at which the 'buffer' of eroded sediment in front of the dune foot degrades during the erosion event increases then and likewise the erosion rate. Therefore, infragravity waves should be taken into account when calculating the amount of dune erosion (Corps of engineers, 1989; Butt and Russell, 1999; McCall, 2008; Ruessink *et al.* (2012); Van Gent *et al.* 2008).

2.1.4 Alongshore variation

The cross-shore dune erosion processes that have been described in section 2.1.2 can be influenced by alongshore processes. These processes may locally reduce or amplify dune erosion during a storm. As a consequence not the whole width of the coast is affected to the same extent; some areas might be structurally eroding (erosional hotspots) while only a few kilometres further virtually no erosion or even accretion is observed. Likewise, the degree of erosion at a certain location may vary over time. Research is being done to gain more understanding of the processes responsible for the observed dune erosion patterns (van de Graaff, 2002; Galal and Takewaka, 2011; van Thiel de Vries, 2011).

Alongshore variations in beach and dune erosion are sometimes easily observed, like for example at barrier islands and spits, where one side shows accretion and the other site shows erosion. But also if a beach seems to be quite uniform, there might be small features that can cause local differences in dune erosion during storms, like variations in the dune height and intersections in the dunes due to notches and swirl holes. These dune characteristics determine how much sand will be supplied to the beach during the storm and therefore how the beach profile will develop (van Thiel de Vries, 2011). Furthermore, it has been found that areas with steeper slopes experienced more erosion due to higher run-up elevations (Sallenger, 2000; Stockdon et al., 2007). Ruessink and Jeuken (2002) found that alongshore variability can be related to beach width.

Other factors that have been shown to result in local variations in dune erosion are the availability of sediment, the wind and wave climate and the degree of vegetation (Carter, 1989; Davidson-Arnott, 2010). Alongshore variability might also be present as non-uniform features in the bathymetry, which is even less obvious. These non-uniform features, like sand bars that are intersected by rips and beach cups, may influence the transformation of the landward propagating waves locally and consequently the dune erosion intensities (van Tiel de Vries, 2009, 2011). Wetzell *et al.,* (2003) also showed that locations with severe erosion can be correlated to special variations in the wave runup around Cape Hatteras. Galal and Takewaka (2011) showed that alongshore differences in cross-shore energy flux and smaller scale changes associated with ridges in front of the coast at a depth of 20 to 30 metres can be related to large scale alongshore variability.

The alongshore variatio processes should be included in assessment tools, because this will improve dune erosion predictions and thereby enhance coastal safety.

2.2 XBeach

2.2.1 Model formulation

XBeach is an abbreviation for eXtreme Beach behavior. It has been designed to compute the natural coastal response, in both the cross-shore and the long-shore direction, during time-dependent severe storm and hurricane conditions. Xbeach is a process-based model, which means that it models the most important processes that force the coastal response. The physical relations that are used for these calculations are based on field observations and laboratory experiments. All processes are averaged over the vertical and solved on a wave group time scale (Roelvink *et al.* 2009, van Thiel de Vries, 2009; Splinter and Palmsten, 2012).

The processes that are modeled in Xbeach can be divided in four different regimes; the swash regime, collision regime, overwash regime and inundation regime (Roelvink *et al.,* 2010). These regimes are based on the Storm Impact Scale system that was invented by Sallenger (2000). This study

will mainly focus on the swash- and the collision regime, because these are the regimes that are concerned with dune erosion. The other regimes are related to overwash and breaching.

In Roelvink *et al.* (2009, 2010) a detailed description is given of the mathematical model, therefore I do not go into detail here, but I will give a short overview.

Grid

The axes in XBeach are always chosen with respect to the coastal area that will be modeled. The x-axis (x) is chosen approximately perpendicular to the coastline and the y-axis (y) parallel to the coastline. The conservative quantities, like the energy, water level, bed level, water depth and concentrations are calculated in the cell centers and flux related parameters like velocities, sediment transport and radiation stress are defined in the cell interfaces (Roevink *et al.*, 2009; Xbeach manual).

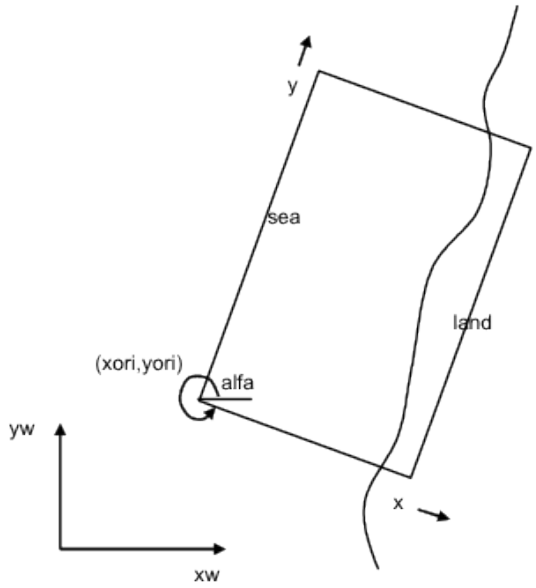

Figure 2. Coordinate system XBeach. (*Roelvink et al., 2010*)

Hydrodynamic forcing of XBeach

Xbeach requires offshore wave boundary conditions. These can be given as a JONSWAP spectrum or SWAN spectrum among others. The wave frequency spectrum is described by a single representative frequency. The transformation of the short waves over the coastal area in the landward direction is described by a time depended version of the wave-action balance. It is used to solve the wave forcing for the shallow water momentum equation and it is solved on the wave group time scale (McCall, 2008; Roelvink *et al.,* 2009; van Thiel de Vries, 2009).

The total wave energy dissipation D for non-stationary waves is obtained using a formulation of Roelvink(1993)

$$D = 2\alpha f_{rep} E_W Q_b \qquad (1)$$

And for stationary waves Roelvink(1993)

$$D = 2\alpha f_{rep} E_W Q_b H_{rms} / h \quad (2)$$

Where α is a coefficient in the order 1, f_{rep} is the representative intrinsic frequency in *Hz*, E_w the total wave energy summed over all directional bins in N/m, H_{rms} the rms wave height and h the local water depth. Q_b is a fraction that describes the transition between no breaking (Q_b=0) and full breaking (Q_b=1) and the ratio between the local wave height and depth, given by :

$$Q_b = \min[1 - e^{-(H_{rms}/\gamma h)^n}, 1] \quad (3)$$

where n and γ are free model parameters that can be used to calibrate the model.

A roller is generated when the waves break and the momentum that they carried is transferred to the wave column. A roller energy balance is used to compute these transitions. If infragravity waves are predominant, the wave and roller equations should be solved in non-stationary, wave-group mode (McCall, 2008; Roelvink *et al.*, 2009; Roelvink *et al*., 2010). The wave-induced momentum results in radiations stresses that force near shore flows and currents. These flows, which vary on a waves group time scale, are used in the nonlinear shallow water equations and they account for the long wave motions.

The short waves and the rollers induce a wave group varying mass flux. This also contributes to the long wave motions and the return flow in the surf zone. This return flow, which is called the undertow, is very important concerning the seaward sediment transport (see also section 2.1.2). The mass fluxes are derived from the depth-averaged Generalized Lagrangian Mean formulation (GLM). The cross-shore Lagrangian velocity which is calculated as the distance a water particle travels in one wave period divided by the wave period. The Lagrangian velocity is related to the Eulerian velocity which is the velocity observed at a fixed point and the Stokes drift. The bottom shear stresses that result from the return flows are calculated using these Eulerian velocities (Roelvink *et al*., 2010; Splinter and Palmsten, 2012).

Sediment transport

The calculated hydrodynamic processes described above are used to calculate the sediment concentrations in the water column. The subaqueous sediment transport is modelled based on these concentrations using the advection diffusion formulation of Galapatti (1993). The bed elevation evolves as a function of the gradients in the sediment transport.

Dune erosion

The exact processes that affect the release of sand from the dune face, as the result of the near shore hydrodynamics, are still largely unknown. Therefore it is not yet possible to use a process-based description of dune erosion in XBeach (Roelvink *et al.*, 2009). Other models often obtain the behavior of the dune front by extrapolating the wet profile behavior and underwater offshore transport to the dry dune front. In XBeach, the dune face itself is triggered by the near shore hydrodynamics. This is possible because XBeach resolves the long-wave swash motions explicitly. An advantage of this approach is that it is applicable to model dune erosion in two dimensions (McCall, 2008; Roelvink *et al*, 2009). XBeach uses an empirical algorithm. This algorithm is based on experimental results that proved the existence of a linear relationship between the wave impact and eroded dune volume. These experiments were performed by Van Thiel de Vries (2009) in the Delta-flume.

The avalanching in this algorithm is controlled by a critical wet slope (*wetslp*), critical dry slope

(*dryslp*) and a user specified water depth at which the transition is made between the wet and the dry slope (*hswitch*). In adittion, a maximum erosion rate *dzmax* per grid cell can be specified. Avalanching is introduced when the critical wet slope between two adjacent points on the grid is exceeded. This may happen when a dry slope is submerged, because the critical wet slope is smaller than the critical dry slope. When this happens, the amount of sediment that is needed to stabilize the slope is exchanged between the grid points. However, the exchanged amount is restricted to the maximum erosion rate. Setting a maximum avalanching transport rate ensures numerical stability, but it should be chosen high enough so that it does not influence the actual process outcome (McCall, 2008; Roelvink *et al.*, 2009; Brandenburg, 2010).

The critical wet slope should be smaller than the critical dry slope because inundated areas are much more prone to slumping. Default values for the dry and the wet slope are respectively 1 and 0,3 [-] (Roelvink *et al.,* 2009). Thus avalanching starts when two adjacent stable dry points become wet during wave run-up and the critical wet slope is exceeded, for example when the dunefoot is inundated by a large infragravity wave. The adjustment of sediment between the grid points will likely cause a chain reaction in subsequent time steps in the seaward direction, where the eroded sediment is transported away by the infragravity backswash and undertow. It may also cause a chain reaction in the landward direction when the highest wet point is lowered and the slope between this point and the dry point above it exceeds the critical dry slope (Roelvink *et al*, 2009).

It is very important to choose the right magnitude for the parameters controlling the dune face erosion. Brandenburg (2010) did a sensitivity analysis of these parameters, which shows that the amount of erosion is very sensitive to the avalanche parameters that determine the critical wet slope and the maximum erosion rate and less sensitive to parameters critical dry slope and the specified water depth.

Feetback mechanism

The bathymetry changes during the storm conditions due to the changes described above until it is in equilibrium with the storm conditions as explained in sections 2.1.2. This new shape has a negative feedback on the hydrodynamic forcing and therefore the dune erosion rate decrease in time.

3. Hydrodynamic calibration and validation

3.1 Data

The study area was located some 3 km to the south of Egmond aan Zee. The total study area reached alongshore from 500 m north to 40 m south of a local video observation tower. In this area the beach width was around 40 m and the dunes were some 20 m high. Following a cross-shore profile landward one encounters an outer subtidal sand bar, an inner subtidal sand bar and an intertidal sand bar. The cross-shore location and the elevation of the sand bars and troughs varied alongshore and in time. An offshore wave buoy provided the offshore wave spectra data. This buoy is located approximately 18 km to the south of Egmond aan Zee, in front of IJmuiden, at a water depth of 26 meters. It recorded the Hm0 wave height in m, the wave period in s and the wave direction in degrees every 10 minutes. A nearby tidal station also measured the water level with respect to the Dutch Ordnance Datum (NAP), which is about mean sea level, every 10 minutes, which includes both the astronomical tide and the surge.

The height of the shoreward propagating waves decreases when the waves break in the shallower water near the coast. Data on the cross-shore wave transformation in the intertidal zone was collected from September 27 until November 2, 2011 (Brinkkemper, 2013). The instruments were placed on a cross-shore transect over the intertidal sand bar, over a distance of 80 meters. The measurement array contained nine pressure gauges (OSSI, Ocean Sensor Systems Inc.), an electromagnetic flowmeter (EMF), to measure cross-shore and alongshore current velocities, and three mini-frames also equipped with a pressure sensor. All the data were collected with a frequency of 4Hz, except for the OSSI pressure sensors which collected at a frequency of 5 Hz. Additionally, the bed level was measured every day along the transect, unless it could not be reached due to strong winds. More information about the field campaign can be found in Brinkemper (2013).

We converted the measured pressures, induced by the water column above the sensors, to the corresponding water level above the sensors. We obtained the total water level above the bed by adding the level of the sensor above the bed. When a sensor gets submerged under the bed it will still measure the pressure, but the additional pressure due to the sand column above the sensor has to be subtracted from the total pressure in this case, before converting it to the water level above the bed. We estimated the significant Hm0 sea swell or short wave height (Hm0,ss) from the wave spectrum that was derived from the high frequency pressure fluctuations. The low frequency pressure fluctuations are used to calculate the infragravity wave height (Hm0, inf).

3.2 Model setup

Analysis of the wave buoy data shows that two storms passed during the measurement period from 27 September until 2 November 2011. Figure 3a and b show that the measured water level clearly exceeded the predicted astronomical tide between 5 until 7 October and 17 until 19 October, due to the storm surge caused by the two storms. From these records, a total of 8 high water periods were selected, 4 during each storm. We used one of these high tide periods for the hydrodynamic calibration and all periods for the hydrodynamic validation. Every period had a duration of 2 hours, 1 hour before and after high water. We assumed that the water level, wave height and angle of wave incidence were stationary during these periods. The selected periods are shown in figure 3 in magenta. Figure 3c and d

show the Hm0 wave height for both storms. The offshore wave conditions were also averaged over the selected high tide periods, because they did not change significantly during the selected two hours.

The wave conditions were used to create a JONSWAP spectrum (instat 4) for the simulations with a directional spreading of approximately 15 degrees. XBeach uses this spectrum to create the wave conditions at the offshore boundary. The mean wave direction varied per period, from west to north-northwest during the first storm (periods 1 to 4) and from west-southwest to northwest during the second storm (periods 5 to 8). The surge levels varied from 1 m to 1.5 m, the wave heights from 2.5 m to 3.8 m and the wave periods from 6.2 s to 7.8 s. Refer to Table 1 for the values per period. We performed all the simulations that focus on the hydrodynamics without the morphological module. Furthermore, we used Neumann boundary conditions on the lateral boundaries. For a detailed list of settings we refer to appendix A.

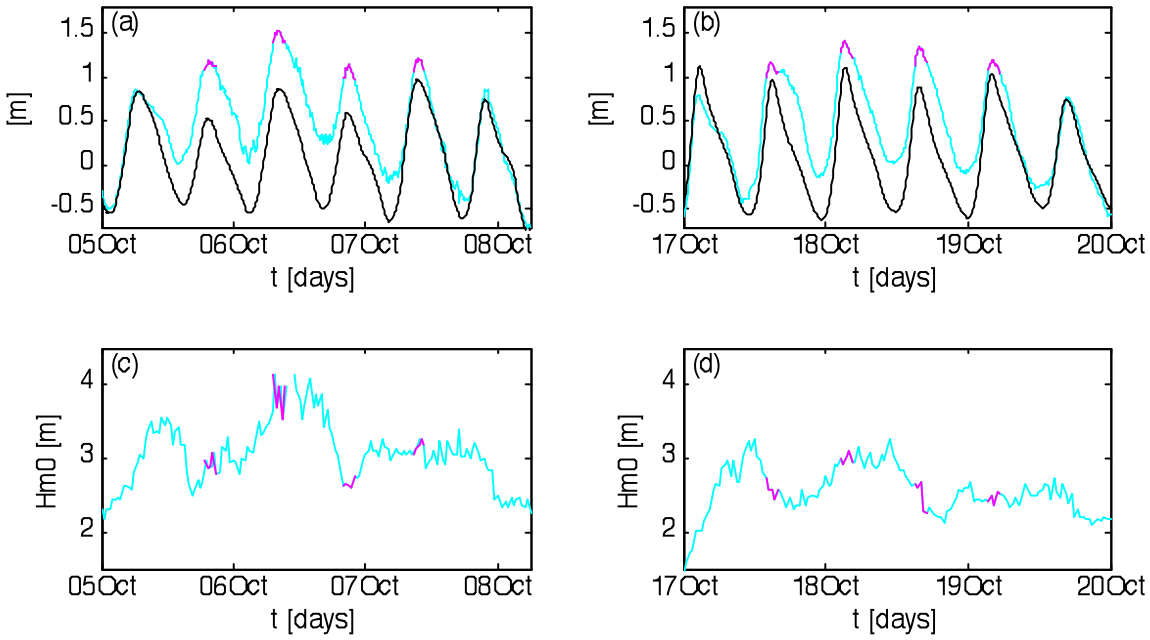

Figure 3(a) and (b) show the predicted astronomical tide (black) and the observed water level (cyan) for the first- and the second storm respectively. (c) and (d) The Hm0 wave height (cyan) for the first- and the second storm respectively. The selected high water periods are indicated in magenta.

	Mean wave direction [°]	Mean surge level [m]	Mean wave height [m]	Mean wave period [s]
Period 1	272.72	1.13	2.93	6.41
Period 2	274.20	1.46	3.84	7.21
Period 3	304.84	1.06	2.65	6.88
Period 4	324.53	1.15	3.17	7.81
Period 5	345.04	1.09	2.56	6.24
Period6	269.90	1.32	3.00	6.46
Period 7	292.25	1.26	2.51	6.79
Period 8	316.63	1.13	2.46	7.10

Table 1. Mean wave conditions per period, which are used to create the wave conditions at the offshore boundary.

The bathymetries that we used for the hydrodynamic calibration and validation are based on daily measured profiles along the measurement transect in the intertidal zone during the field measurement campaign (Brinkkemper, 2013). These profiles were combined with ship survey data to include the offshore bathymetry. The field measurement campaign was held from September 27 until November 2, 2011, while the ship survey data date back from the beginning of November. Therefore some uncertainty in the offshore bathymetry has to be taken into account. They could unfortunately not measure the bed level in the intertidal zone every day during the first storm due to the rough conditions. Therefore the only available profile for the first 4 selected high water periods was the profile measured on the last day of the first storm. During the second storm daily measurements were available. Figure 4 shows a cross-shore profile of the dune foot and the inner sub-tidal and intertidal sand bars with the different bottom profiles measured in the intertidal zone. The downward pointing triangles indicate the locations of the pressure sensors.

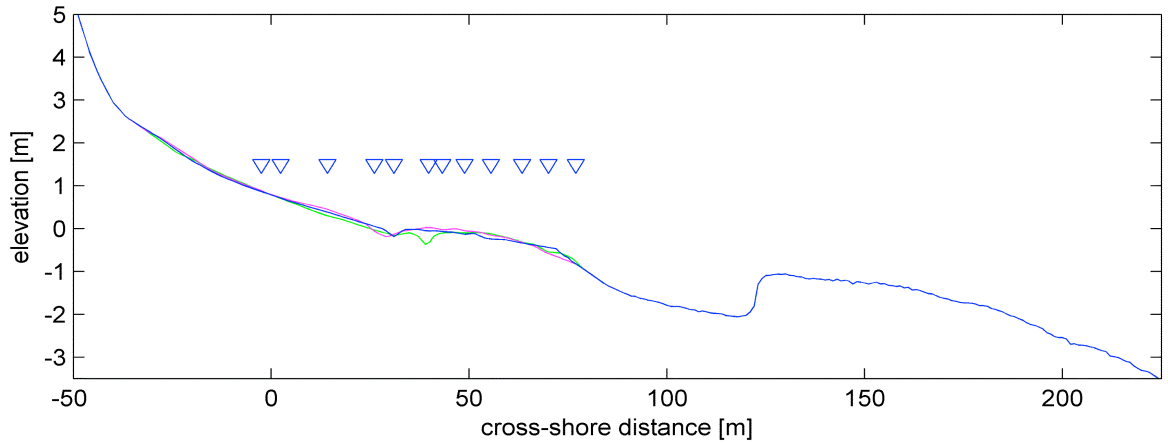

Figure 4. The cross shore profiles composed of a ship survey measurements and the bed profiles measured along the measurement transect during the field campaign on October 8 (green), 18 (magenta) and 19 (blue). The triangles denote the locations of the pressure sensors.

We chose high water period 5 for the hydrodynamic calibration, because there was a bed level measurement available from the same day and the angle of wave incidence was not close to shore normal. We setup a 1D model for the calibration using the corresponding profile with the bed measurement from October, 18.

Additionally we setup 2D models for the validation, with uniform topographies based on the cross-shore profiles that correspond to the selected periods. The topographies covered an area of 1120 m alongshore and 1764 m cross-shore. The applied grid had variable cell sizes; dy was 20m outside- and 5 m on the inside the center of the study area. The grid was also non-uniform in the cross shore direction, coarser offshore and finer towards the shore, with a maximum cross-shore cell size (dxmax) of 7.6 m and a minimum cross-shore cell size (dxmin) of 1 m. The grid size is important because to large gradients between grid cells will lead to energy loss during the computations, but if the grid is to fine energy will be lost due to numerics, and computation time increases rapidly with the amount of grid cells.

3.4 Calibration

We calibrated the hydrodynamic forcing of XBeach by minimizing the root mean square (ε_{rms}) between the predicted and the observed short wave transformation in the intertidal zone for period 5. The calibration focussed on adjusting the parameters n and γ in the wave energy dissipation formulation of Roelvink (1993) described in section 2.2.2. γ was varied between 0.40 and 0.90 and n was varied between 5 and 20. Figure 5 shows the ε_{rms} values obtained by comparing the observed and predicted Hm0,ss wave height above the measurement locations. The Hm0, ss is more sensitive to n and γ then the Hm0, inf. If we only look at the Hm0, ss the best model agreement was found for γ = 0.55 and n = 5. However, this does not good results for the infragravity waves. Furthermore 2D simulations showed that the Hm0,inf wave height is underestimated for values of $\gamma < 0.55$ and $n < 10$. The reason for this is that the wave groupiness is suppressed for smaller n leading to underestimation of the long waves. This is unfavourable, because long waves play an important role with regard to dune erosion (section 2.1.3). Considering these limitations, the best model agreement is found for γ = 0.55 [-] and n = 10 [-], which are the default values.

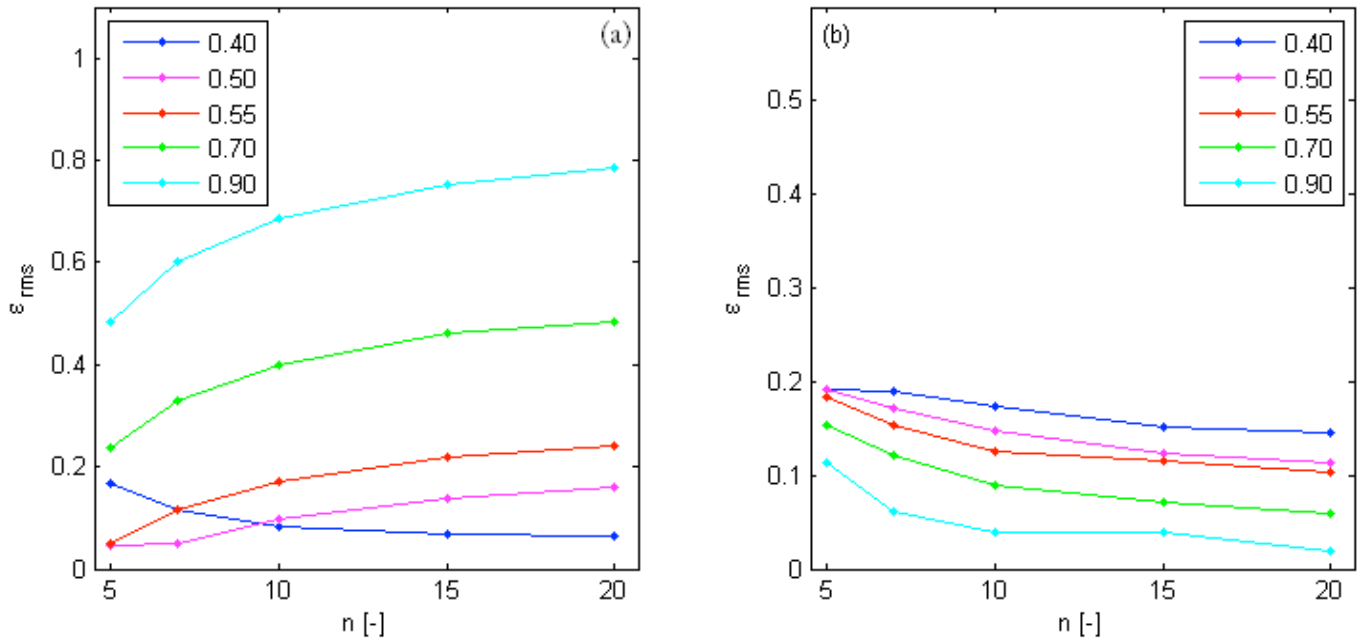

Figure 5. The root mean square (ε_{rms}) values that were obtained by comparing the predicted and observed short wave transformation in the intertidal zone for different values of γ and n.

3.5 Validation

For the hydrodynamic validation we compared the predicted and observed landward Hm0,ss and Hm0,inf wave height transformation for the seven different periods. We used the 2D model setup described in section 3.2 and the calibrated hydrodynamic settings. Xbeach applications for dune erosion under natural conditions are often (partly) carried out in 1D profile mode (Roelvink *et al*., 2009; Van Thiel de Vries, 2009; Splinter and Palmsten, 2012). We specifically chose to use the 2D mode however, because this leads to better predictions of the Hm0,inf wave height.

Figure 6a and b shows the predicted against the observed Hm0,ss and Hm0,inf wave height respectively. The Hm0,inf was reasonably well predicted, but the Hm0,ss was over predicted. The over prediction is the strongest when the waves enter the intertidal zone and decreases shoreward with decreasing wave height. The calculated errors are shown in table 1. An explanation for the overprediction of the short waves could be that the outer bar was higher in reality than in the used bathymetry, because the offshore bathymetry was measured later than the intertidal wave transformation data.

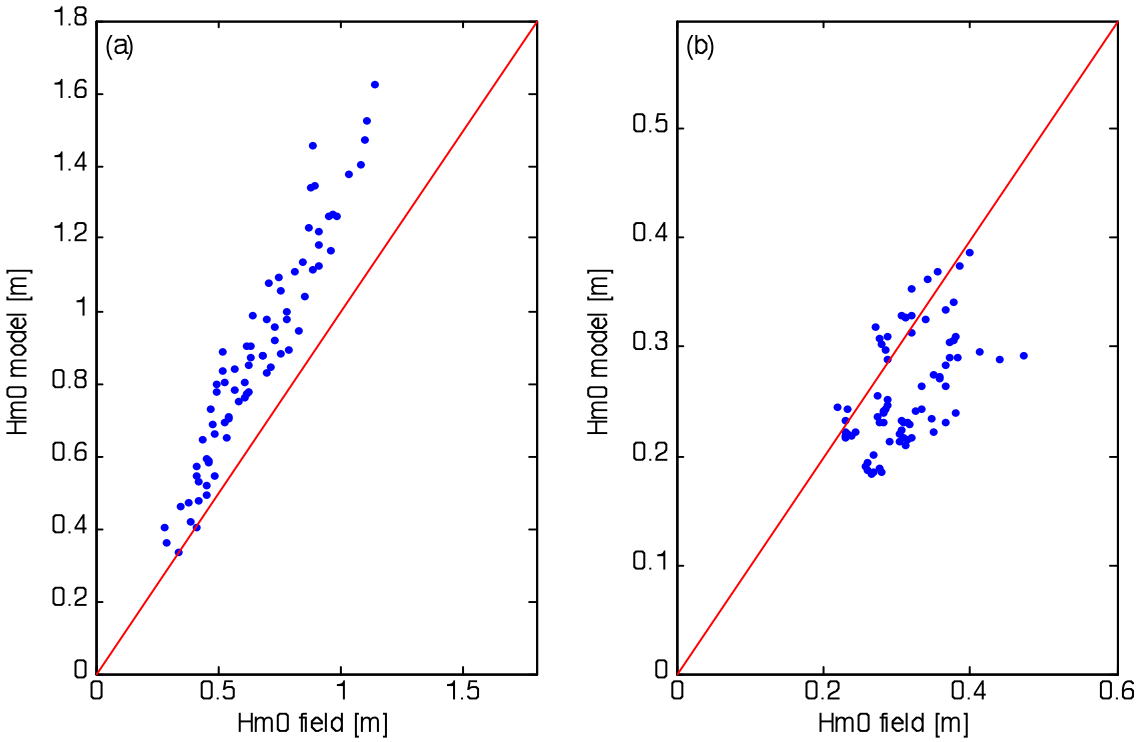

Figure 6. The observed against the predicted Hm0,ss in (a) and the Hm0,inf in (b) for the 2D mode.

	Short waves	Infragravity waves
root mean square (ε_{rms}) [m]	0.086	0.043
Lineair regression (r^2)	0.92	0.29
Slope best fit line	1.4	0.52

Table 2. The quantified errors for the results of the validation performed in 2D mode.

Comparison of figures 6 and 7, which show the modeled Hm0,ss and Hm0,inf wave height versus the observations for the 1D and 2D mode respectively, shows that the Hm0,ss wave height was almost unaffected by the changed mode, but the Hm0,inf wave height was less well predicted in the 1D mode. We recommend using the 2D mode instead of the 1D mode, because the errors are bigger for the one 1D mode; the wave height is more often underestimated (compare tables 1 and 2).

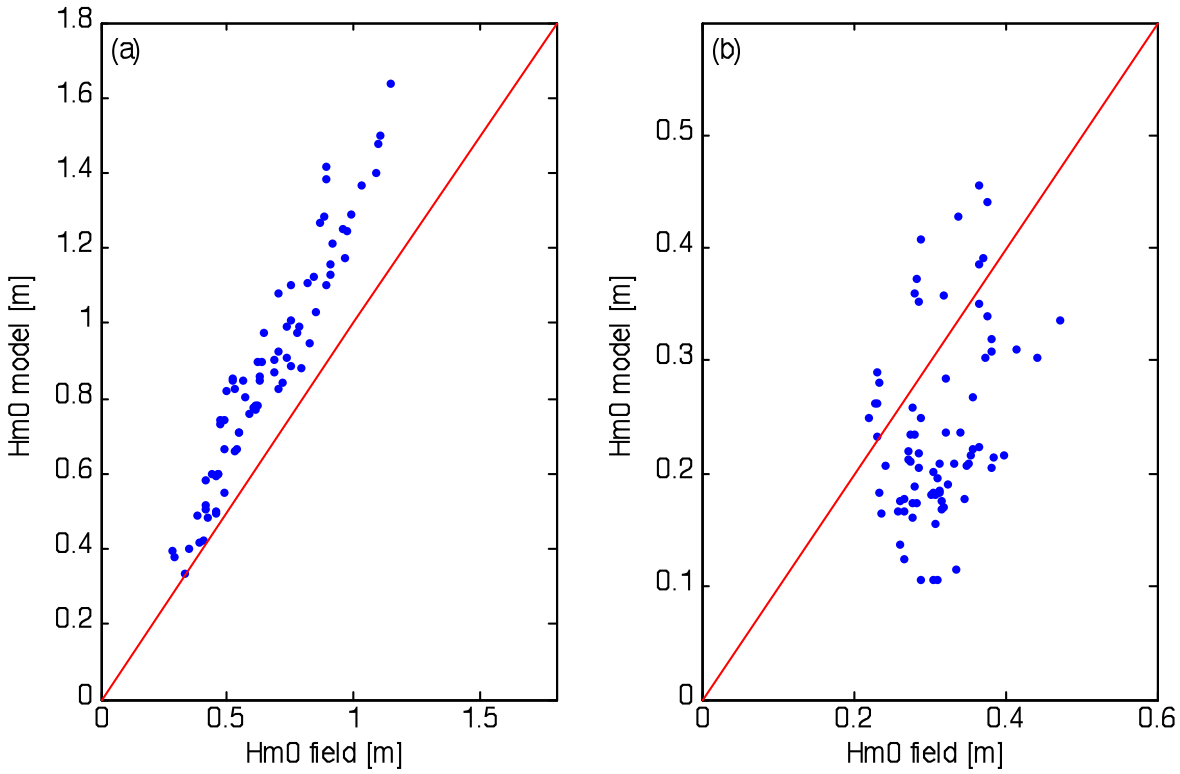

Figure 7. The observed against the predicted Hm0,ss in (a) and the Hm0,inf in (b) for the 1D mode.

	Hm0,ss wave height	Hm0,inf wave height
root mean square (ε_{rms})	0.085	0.077
Lineair regression (r^2)	0.92	0.12
Slope best fit line	1.4	0.55

Table 3. The quantified errors for the validation performed in 1D mode.

4. Morphological validation

4.1 Method

To answer the second main question; how do XBeach simulations compare to field observations of dune erosion and the alongshore variation thereof, XBeach was morphologically validated based on a dune erosion event observed between 3 and 6 January, 2012. For the validation we compared trends in the observed and predicted dune erosion, like the highest point on the dune face affected by erosion, the slope of the dune face before and after the erosion event, the dune foot retreat and the eroded volume. Thereafter we explored the causes of the alongshore variability in these trends.

4.2 Observation

4.2.1 Wave forcing

The offshore wave conditions, used for the morphologic validation, were derived from the same wave buoy as the one used in the hydrodynamic calibration and validation. Furthermore we used the water level measured with respect to the Dutch Ordnance Datum (NAP) by a nearby tidal station (more details were given in section 3.2). Figure 8 shows that the storm, which caused the dune erosion event, was accompanied by 5-m high waves and that high tide storm surge superimposed on the high tide water level led to a increase in water level up to 2 m above NAP.

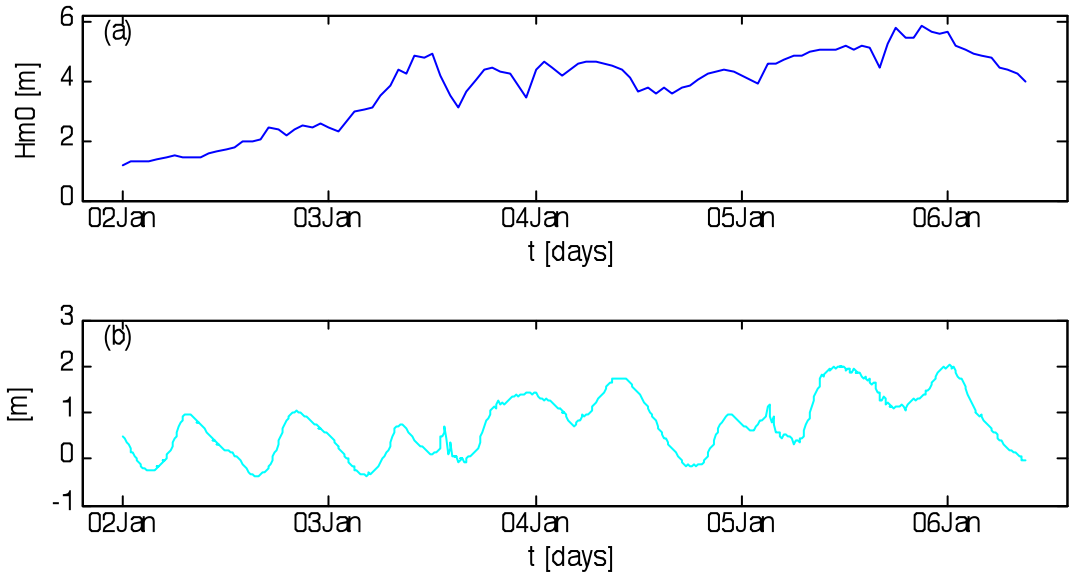

Figure 8 (a) The Hm0 wave height and (b) the water level both in m with respect to the Dutch Ordnance Datum (NAP) during the storm period.

The images from the video tower show that the dune erosion was most pronounced during the last two high tides. It was however not possible to distinguish between those tides because it is only possible to estimate the amount of erosion during low tide when it is light outside and that was not the case.

4.2.2 The topography observed before the storm

The beach and dune topography were measured with a terrestrial laser scanner, 2,5 months before- and 5 days after the dune erosion event. The result of the laser scan measurement was a 3D point cloud. Points that were not reflections of the topography were removed. Additionally, we reduced the large amount of points was by placing them on a grid and averaging them per 0.2 m by 0.5 m grid cell. Linear interpolation was used to fill any empty cells.

Figure 9 shows the topography observed before the dune erosion event. The dune row closest to the beach was about 20 m high and the beach was generally some 60 m wide (measured between the dune foot at 3 m and the shore-line at 0 m with respect to the Dutch Ordinance Datum). Figure 10 shows the angle between the dune face observed before the dune erosion event and the horizontal. This angle varied between 20 and 28 degrees.

The observed topography includes the intertidal bathymetry, because the measurements were performed during low tide. An intertidal sand bar is visible between approximately y = -500 m and y = -300 m and x = 30 m and x = 60 m and to the south of this sand bar, around y = - 175, there is a deeper area. Furthermore, an embryonic dune field was observed in the area between approximately y = -500 m and y = -340 m and x = -55 m and x = -42m. Figure 11 shows them in a photograph.

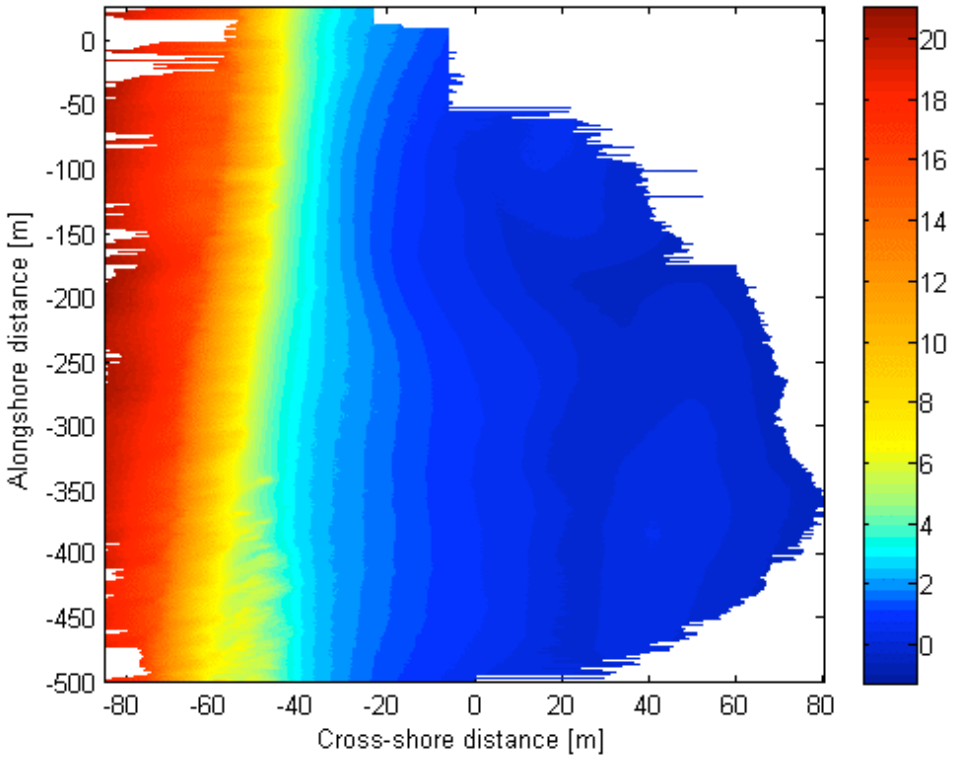

Figure 9. The topographical map observed before the dune erosion event. The colour scale shows the elevation with respect to Dutch Ordinance Datum.

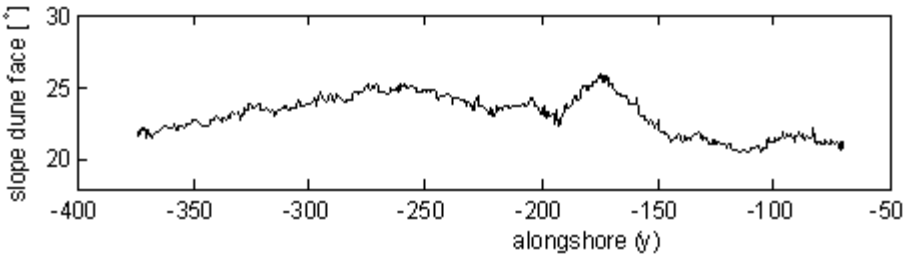

Figure 10. The slope of the dune face before the dune erosion event.

Figure 11. A snapshot, taken in the northerly direction on January 2, from the video observation tower near Egmond aan Zee. The embryonic dune field is marked with a yellow ellipse.

After the dune erosion event multiple scans were made with the terrestrial laser scanner to cover a larger area. These scans were geo-referenced by using reflectors that were placed in the scanned areas and clearly visible on the scans. We removed a little area behind the remains of the embryonic dune field, because they partly blocked the laser beam and therefore it was not measured properly.

Figure 12 shows the topography observed after the dune erosion event. The erosion did not reach the top of the dunes and therefore the height of the first dune row did not change during the erosion event. The width of the beach remained around 60 m in the north, but increased southward from approximately 60 m wide at y = -500 to 80 m wide at y = 300. Comparison of the figures 11 and 13 shows that most of the embryonic dune field eroded during the storm.

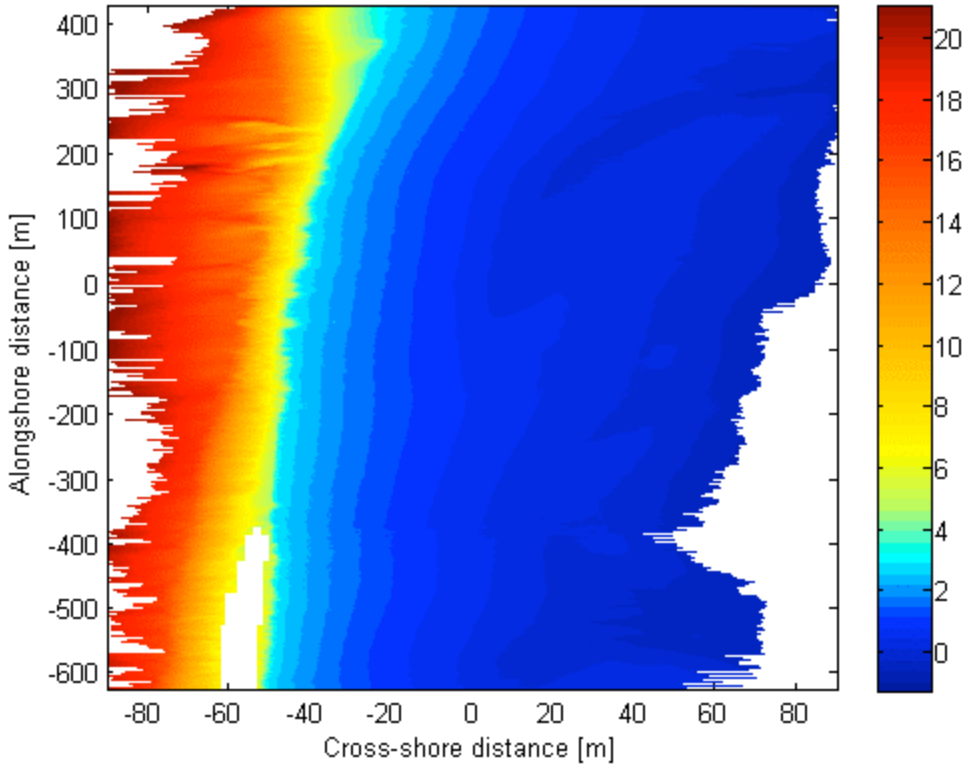

Figure 12 The topographical map observed after the dune erosion event. The colour scale shows the elevation with respect to Dutch Ordinance Datum (NAP).

Figure 13. A snapshot taken in the northerly direction on January 8, from the video observation tower near Egmond aan Zee. The yellow ellipse marks the location where the embryonic dune field was located.

4.2.3 The observed dune erosion

Subtracting the observed post-storm topography from the pre-storm topography gives the topographic difference map shown in figure 14a. Erosion is shown as positive and an increase in elevation is shown as negative in this figure. It can be seen that the amount of dune erosion varied strongly alongshore. The erosion in the area of the embryonic dune field is visible between y = -500 m and y = -340 m. From y = -340 m southwards a minor 1 meter cliff was observed that grew gradually in height up to approximately 6 m around y = -200 m. The cliff can be recognized in figure 14c, which shows the cross-shore profiles observed before and after the dune erosion event at y = -350 m and figure 15a shows a photo of the cliff. From y = -200 southward the height to which the dune face was affected by erosion increased rapidly up to slumping of the entire dune face between y = -150 m and y = 25 m. The cross-shore profile at y = -75 m observed before and after the dune erosion event is shown in figure 14b and figure 15b and c show photo's of this area.

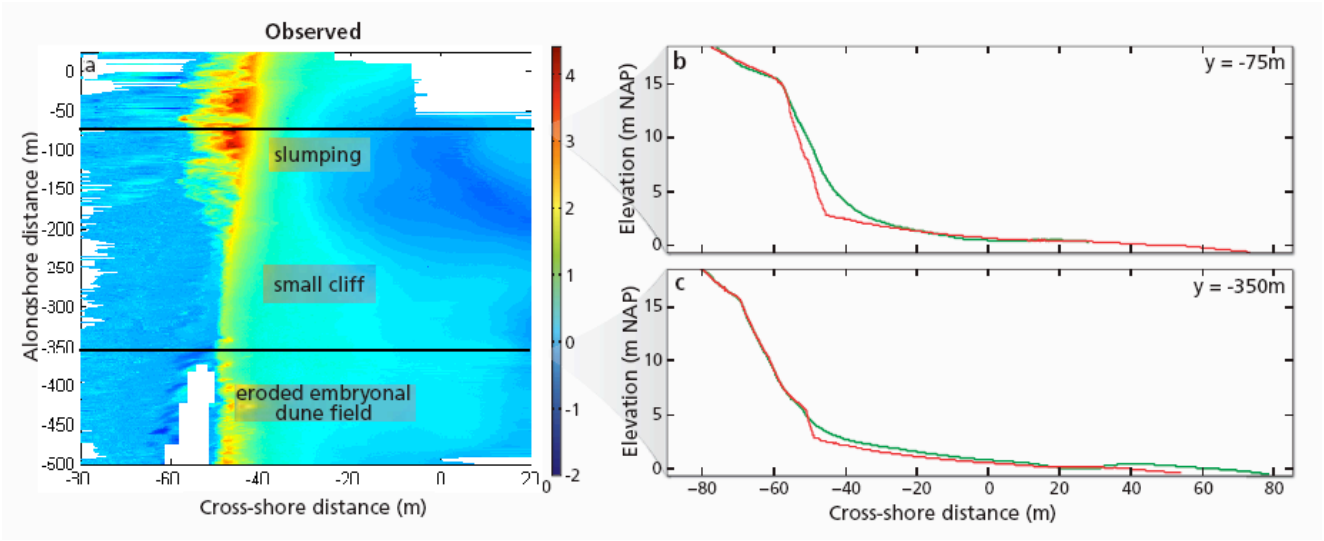

.
Figure 14 (a) The observed topographical difference map and, on the right, the cross-shore profile observed before (green) and after (red) the dune erosion event at (b) y = -75 m and (c) at y = -350 m. The color scale shows the elevation change in meters; erosion is shown as positive.

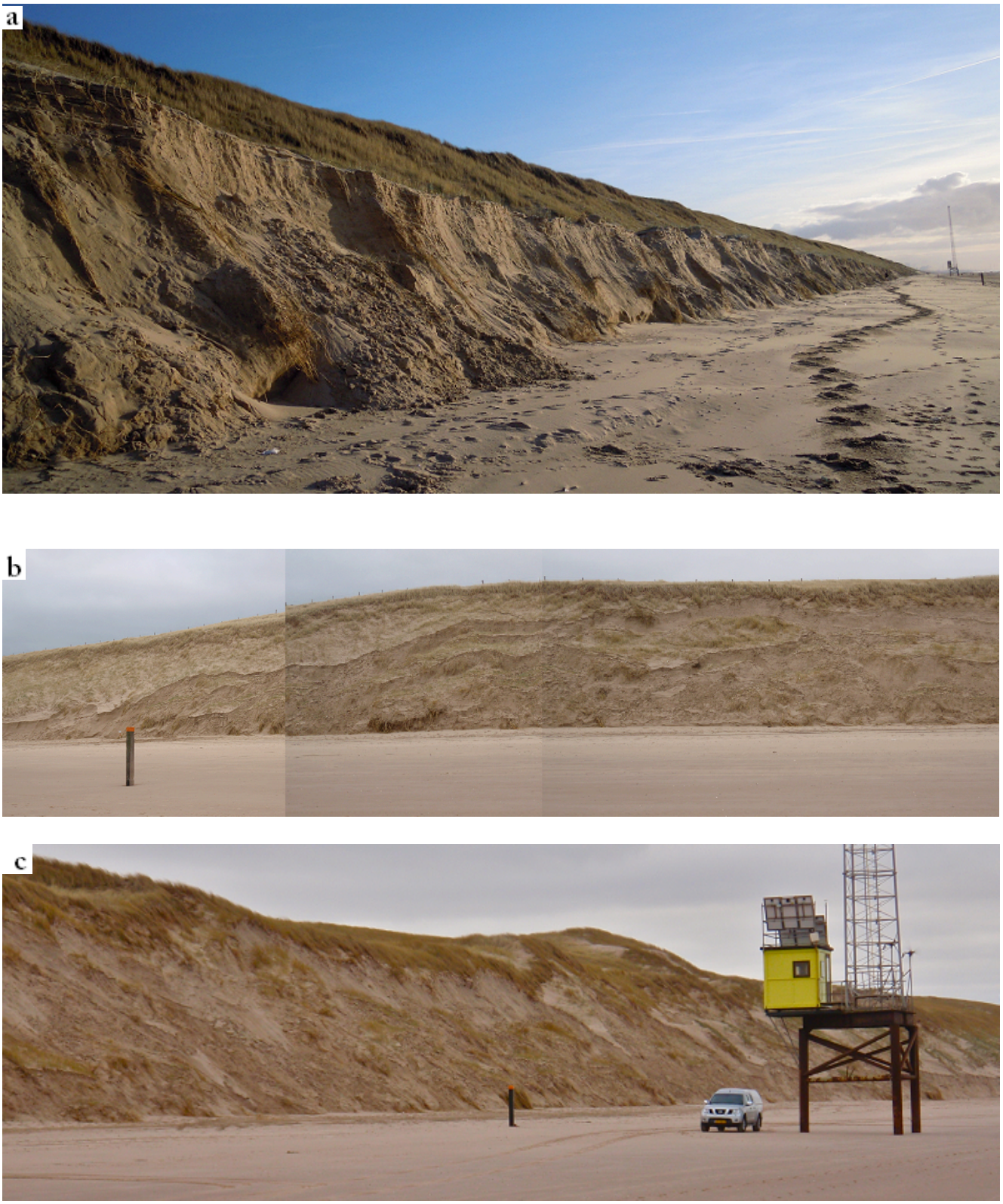

Figure 15. Photos of the dune erosion near Egmond aan Zee. From (a) a cliff upto slumping of the entire dune face in (b) and (c).

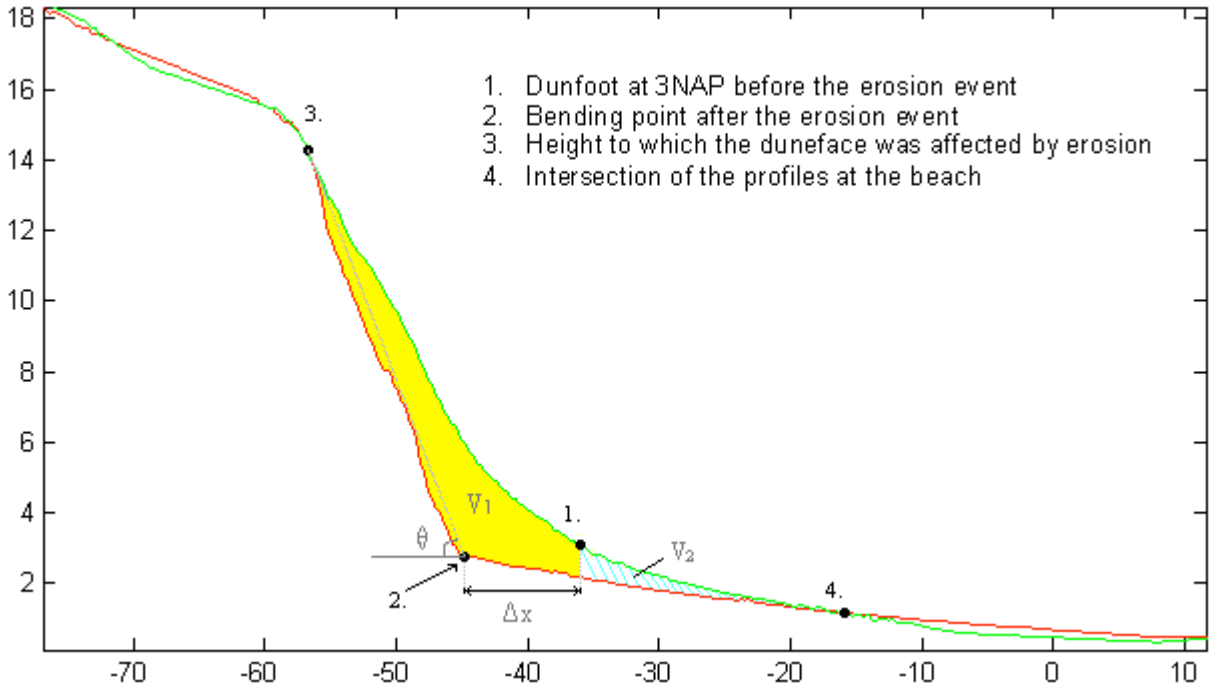

Figure 16. shows the cross-shore profile observed before (green) and after (red) the dune erosion event at y = -75 m with the points that were used to calculate the dune erosion trends per cross-shore profile. Furthermore it shows the angle of the duneface after the erosion event with respect to the horizontal θ, the dune foot retreat Δx and the eroded volume V.

We calculated the highest point on the dune face affected by erosion, the slope of the dune face before and after the erosion event, the dune foot retreat and the eroded volume, using the definitions shown in figure 16. Figure 17 shows the alongshore trends in these features. They could only be calculated northward of y = -375 m, because not enough data were available for the area behind the embryonic dune field. As already described qualitatively in the beginning of this section, the height to which the dune was affected by the erosion (point 3) increased towards the south from approximately 4 m (1 m above the dune foot) to 15 m respect to the Dutch Ordinance Datum (NAP).

The slope of the dune face became steeper in response to the storm. The angle of the dune face observed before the dune erosion event with respect to the horizontal (θ) varied between 20 and 28 degrees and the dune face in the area of the cliff, between y = - 375 m and y = -200 m, observed after the dune erosion event made an 45° degree angle on average with respect to the horizontal. This is equal to the assumption made in the DUROS+ that the erosion profile will have a 1:1 duneface slope for the maximum storm surge level (Brandenburg 2010). The angle with respect to the horizontal was a bit lower in the area with the slumping, 40° on average.

The dune foot retreat (Δx) was rather constant alongshore, around 8 m. It was calculated as the cross-shore difference between the dunefoot at 3 NAP before the dune erosion event (point 1) and the bending point in the cross-shore profile after the dune erosion event (point 2). The eroded volume (V_1) increased from approximately 4 m^3/m at y = -375 m to 47 m^3/m at y = 50 m and then decreased again. This volume was calculated as the area between the cross-shore profiles from the height to which the dune was affected by erosion (point 3) to the dunefoot at 3 NAP before the dune erosion event (point 1) multiplied by the width of the profile (1 m) and divided by 1 m. The dune erosion can also be

calculated as the volume ($V_1 + V_2$), between height to which the dune was affected by erosion (point 3) and the point where the profiles intersect on the beach (point 4) times the width, in order to include the beach erosion, but this leads to a higher uncertainty because the beach topography may have changed between the measurement before the dune erosion event 2,5 months before the dune erosion event and the dune erosion event itself.

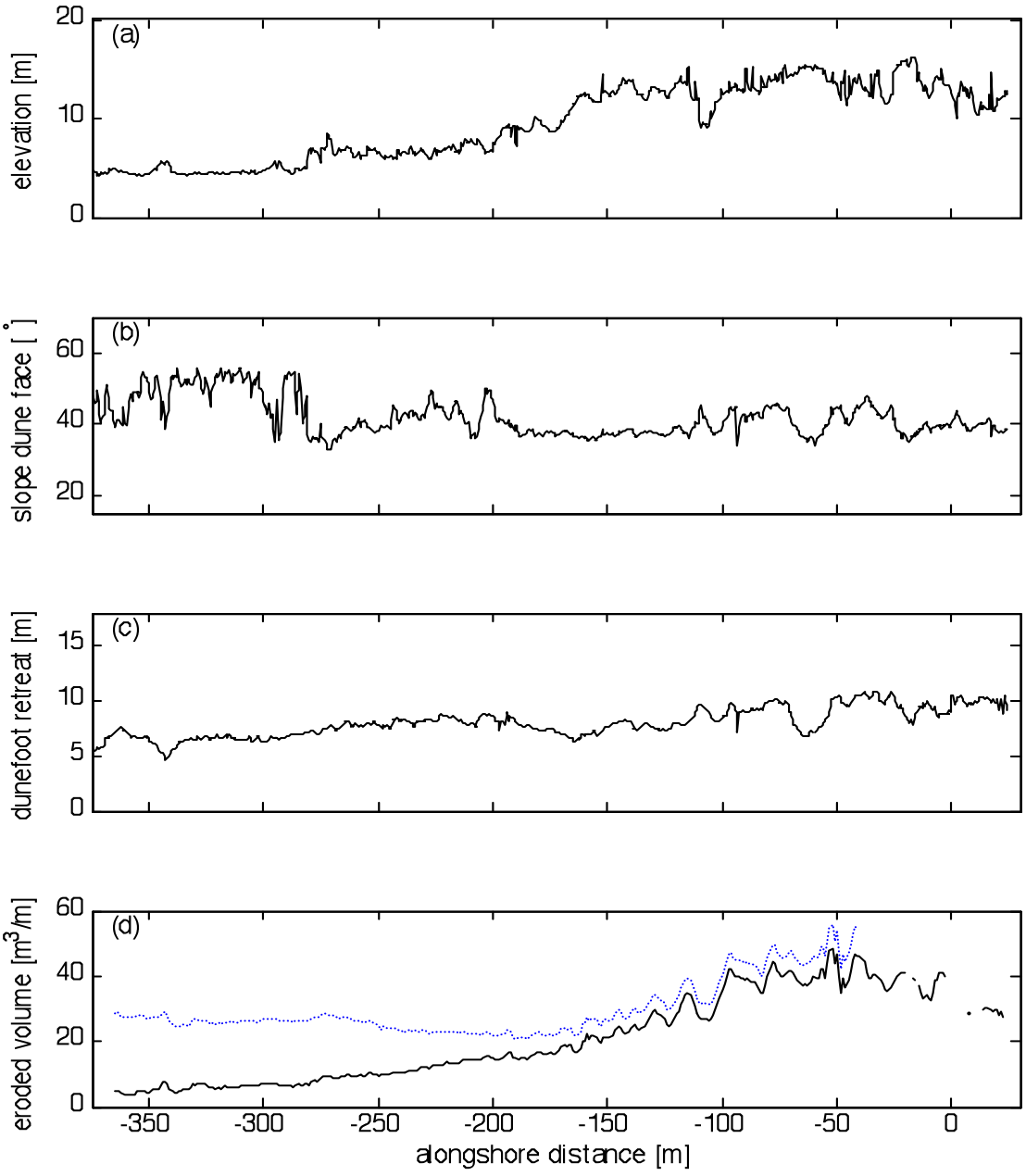

Figure 17. shows the observed alongshore trends in (a) the height to which the dune face was affected by the dune erosion event (b) the angle of the dune face after the dune erosion event with respect to the horizontal (c) the dunefoot retreat and (d) the eroded volume *V1* between the top of the dune face to the pre-erosion event dune foot (black line) and the eroded volume ($V_1 + V_2$) between the top of the dune face and the point on the beach where the cross-shore profiles observed before and after the storm intersect again (striped blue line).

4.3 Model

4.3.1 Model setup

For the morphologic validation we created an Xbeach model using the offshore wave spectra measured during the storm described in 4.2.1, the topography observed before the dune erosion event as described in section 4.2.2 and the calibrated hydrodynamic settings.

The observed topography did not cover the entire bathymetry, therefore it was extended seaward using transect measurements that are part of an ongoing coastal monitoring effort along the Dutch coast. These transect were also used to extend the bathymetry southward to cover the area measured after the dune erosion event. These transect measurements do however not reach further then 2 meter above the dune foot and analysis of the dune erosion was therefore limited to the area measured before the dune erosion event. The resulting bathymetry was extended 1.5 km to both sides in the lateral direction with a uniform area, to eliminate wave shadow in the area of interest. This uniform area was created by copying the row on the lateral boundaries in the lateral direction. The applied grid was uniform alongshore with a cell size of dy = 20 m on the sides and 5 m in the middle area and non-uniform in the cross shore direction, coarser offshore and finer towards the shore, with a maximum cross-shore cell size (dxmax) of 7.6 m offshore and a minimum cross-shore cell size (dxmin) of 1 in the shallower areas.

A time series of JONSWAP spectra (instat 41) was used to set the wave conditions like the wave height, wave period and water level, per time step. The period from January 2 to 6, 2012, 102.5 hours in total, was simulated to obtain the dune erosion predicted by XBeach. We used the calibrated hydrodynamic settings described in chapter 3, which showed that $\gamma = 0.55$ and $n = 10$ are the best settings for those free parameters. The advantage of this calibration was that it reduced the amount of unknown free parameters that could affect the dune erosion prediction. For the morphodynamic settings we used the morphologic parameter settings calibrated by Splinter and Palmsten (2012). They found good model agreement using the default settings for: the threshold depth for the return flow (*hmin)* = 0.01 m, threshold depth for the drying and flooding (*eps)* = 0.1 m, critical avalanching slope under water (*wetslp)* = 0.3, critical avalanching slope above water (*dryslp)* = 1 and the water depth at interface of *wetslp* and *dryslp* (*hswitch)* = 0.1 m.

Only for the parameter which describes the asymmetric transport due to wave asymmetry and skewness (*facua*) better model agreement was found if facua was set to 0.15. Furthermore, Neumann boundary conditions were applied on the lateral boundaries. A detailed list with settings can be found in appendix B for further reference.

4.3.2 Model predictions

Figure 18 shows the predicted changes in dune morphology in response to the storm for different time steps. The dunes eroded most during the last 12,8 hours of the storm according to the model, thus during the last high water. This corresponds to the observations, although from the observations it was not possible to distinguish between the last two high waters (see section 4.2.1).

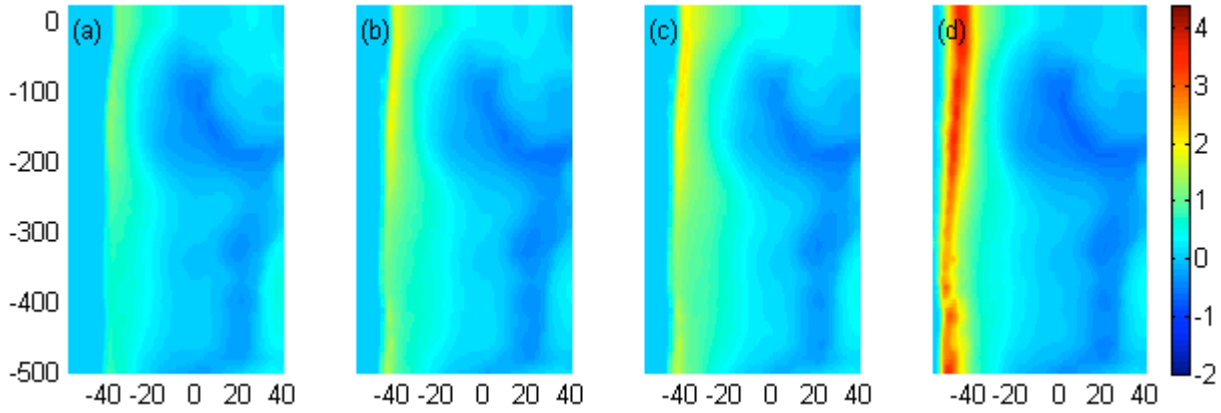

Figure 18. The predicted topographical difference map at (a) t = 64 h, (b) t = 76.9 h, (c) t = 89.7 h, (d) t = 102.5 h.

Figure 19 shows the same graphs as figure 14, but now based on the post-storm topography predicted by the model. Comparison of figures 19a and 14a shows that the predicted dune erosion was overestimated, but that the predicted alongshore variability in dune erosion and elevation of the beach shows resemblance with the observations. A local erosion maximum was predicted between y = - 500 and y = - 400 m, where the embryonic dune field was located and a minimum around y = -350 and from thereon it increased southward again.

Comparison of the observed and predicted cross-shore erosion profiles in figure 19c, shows that the observed bending point between the dune face and the beach was sharper, that the observed dune foot retreated less and that the observed slope of the dune face was steeper then predicted by the model, at y = -350 m, in the area of the cliff. Figure 19b shows that the differences between the observed and predicted erosion profiles was less at y = - 75 m, in the area of the slumping. These alongshore trends are also shown in figure 20. The green lines show the observed dune erosion trends for comparison.

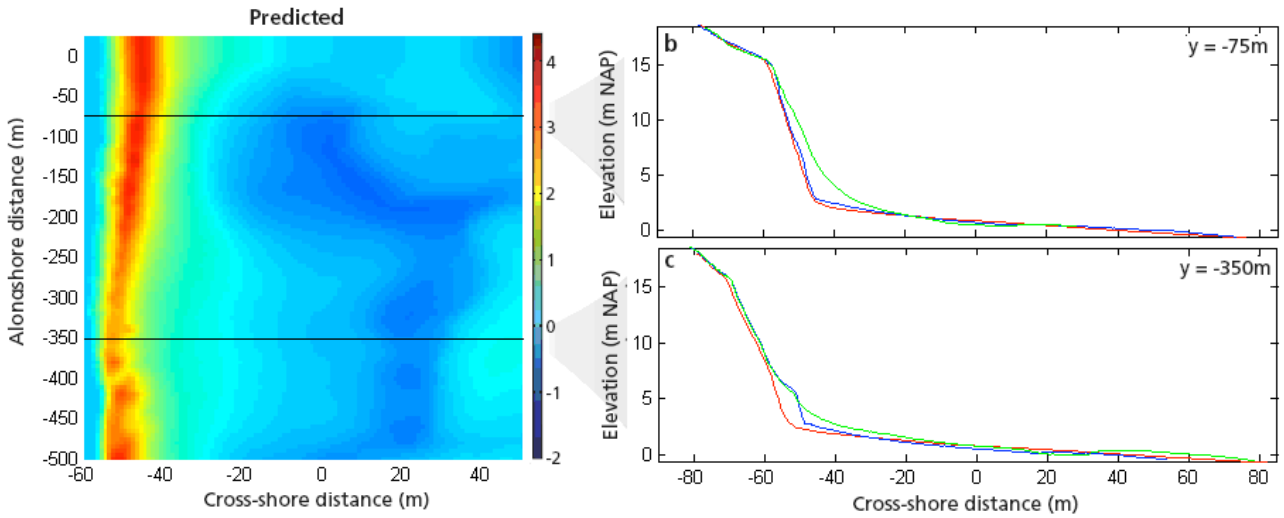

.

Figure 19 (a) The predicted topographical difference map and, on the right, the cross-shore profiles observed before (green) and after (blue) the dune erosion event and the predicted post-storm profile (red) at (b) y = -75 m and (c) at y = -350 m. The color scale shows the elevation change in meters.

We calculated the trends in the predicted dune erosion in the same way as we calculated the observed dune erosion trends (see section 4.2.3). The predicted height to which the dune was affected by the erosion (point 3) increased towards the south, just like it was observed, but from approximately 7 m (4 m above the dune foot) to 15 m with respect to the Dutch Ordinance Datum. The angle of the dune face with respect to the horizontal (θ), was 46 degrees on average, which is 1 degree higher than the assumption made in the DUROS+ model. The dune foot retreat (Δx) was on average 11 m, broadly 3 m further then observed, on average 37% further the average observed dune foot retreat.. The erosion volume (V_1) ranged between approximately 25 m^3/m at y = -375 m to 51 m^3/m at y = 50 m. The total amount of dune erosion in the study area was over predicted with 76% compared to the observations. When the dune erosion was calculated as the volume ($V_1 + V_2$), it varied between 39 m^3/m and 68 m^3/m.

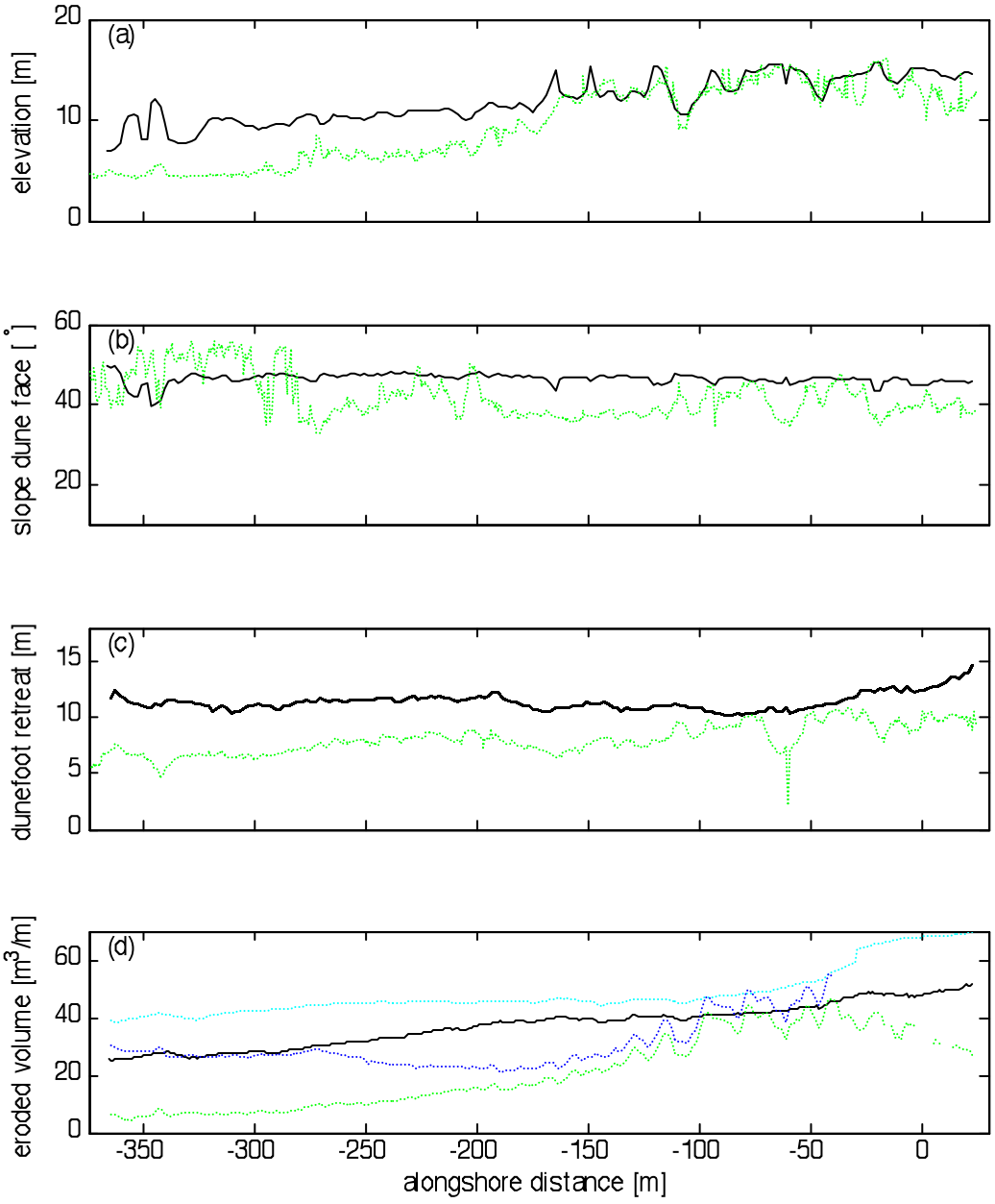

Figure 20 shows the predicted (solid black) and observed (striped green) alongshore trends in (a) the height to which the dune face was affected by the dune erosion event (b) the angle of the dune face after the dune erosion event with respect to the horizontal (c) the dunefoot retreat and (d) the eroded volume $V1$ between the top of the dune face to the dune foot before the erosion event and the observed (striped blue) and predicted (striped cyan) eroded volume ($V_1 + V_2$) between the top of the dune face and the and the point where the cross-shore profiles intersect on the beach.

The observed and modeled dune erosion show broadly the same alongshore variation, but this did not yet explain by what it was caused. To explore the reasons for this alongshore variability, we looked at the influence of the initial topography on the dune erosion predictions. We performed simulations with two additional topographies; one with the observed dune topography but a uniform bathymetry, based on a characteristic bathymetry profile, and one with the observed bathymetry but a uniform dune topography based on a characteristic dune face profile. Additionally, we performed a simulation with the measured pre-storm topography, described in section 4.2.2, as a reference. Figure 21 shows the three topographies. To decrease simulation time, only the last 12 hours of the storm were simulated, because they cover the peak of the storm which caused the most erosion, as explained in the beginning of this section. All the other settings were equal to the settings for the morphologic simulation described in section 4.3.1

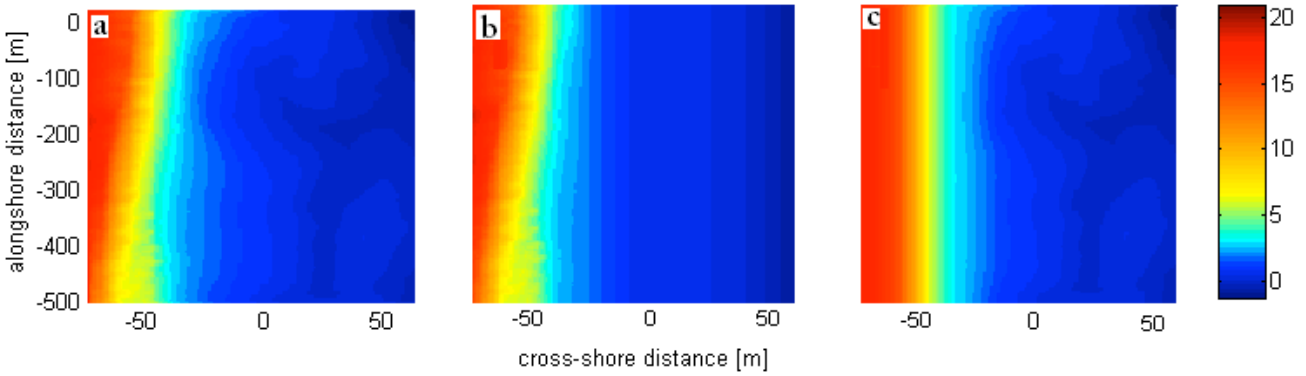

Figure 21. The pre-storm topography (a) as observed, (b) with the observed dune topography but a uniform bathymetry and (c) with the observed bathymetry but a uniform dune topography.

Figure 22 shows the predicted morphological change using topographical difference maps for the three different initial topographies. Generally less erosion was predicted than observed, which could be expected, because the simulation time was shorter. XBeach predicted alongshore variation for all three topographies; therefore the alongshore variation cannot be caused by alongshore variation in only the bathymetry or the dune area.

The erosion predicted based on the reference topography and the topography with the uniform bathymetry both show a local erosion peak between = -500 m and y = -400 m where the embryonic dune field was situated. This peak is not distinct in the topographical difference map predicted based on the topography with the uniform dune area.

The erosion predicted based on the reference topography and the topography with the uniform dune area both show an erosion maximum around y = -100 m, comparable to the observations and the total storm prediction. This maximum is not clear in the topographical difference map predicted for the topography with the uniform bathymetry. Furthermore topographical difference maps also show a similar elevation pattern in the near-shore area. Figure 23 shows the alongshore trends in the highest point on the dune face affected by erosion, the slope of the dune face before and after the erosion event, the dune foot retreat and the eroded volume.

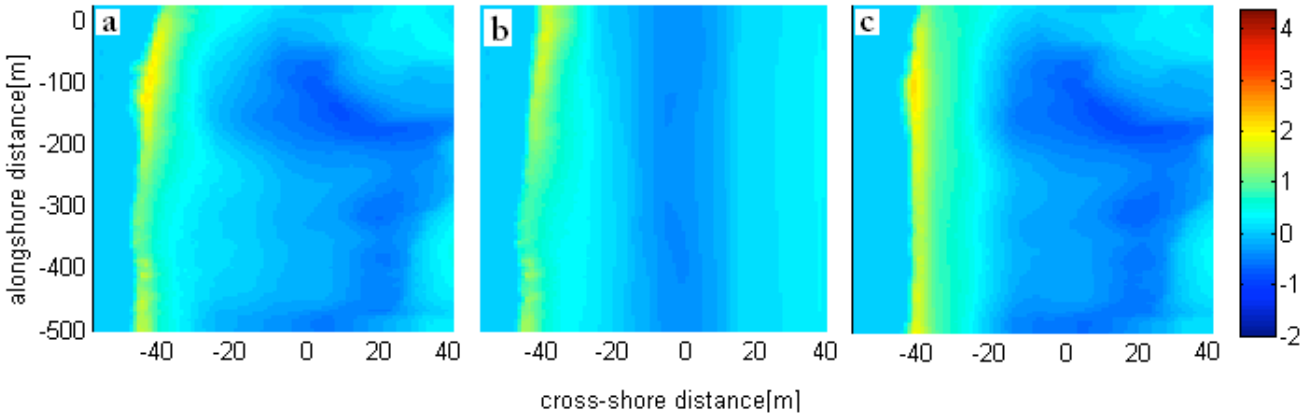

Figure 22 shows the predicted morphologic change during the last twelve hours of the storm with as the initial topography (a) the topography observed before the dune erosion event, (b) the observed topography but with a uniform bathymetry and (c) the observed topography with but a uniform dune area.

For the simulation with the reference bathymetry, the model predicted that the erosion affected the dune face up to approximately 4 m at y = - 350 m and that this height increases to maximum of around 8 m between y = - 150 m and y = -50 and then decreased again to approximately 5 m. The slope made an 45 degrees angle with the horizontal on average and the dunefoot retreat was around 6 m. The eroded volume increased from 5 m^3/m at y = -350 m to a maximum of approximately 16 m^3/m between y = -150 m and y = -50 m and then decreased southward again to approximately 7 m^3/m.

For the simulation with the topography with the uniform bathymetry, the model predicted that the height to which the dune was affected by the erosion also grew southward, from 4 m up to 6 m, but more gradually than for the reference simulation and it does not show a maximum in the south. The slope made an angle of 40 degrees on average with respect to the horizontal between y = -375 m and y = -150 m and 45 degrees between y = - 150 m and y = 25m. The dune foot retreated 5 m on average. The eroded volume grows gradually from 4 m^3/m in the north to 12 m^3/m in the south, but does not show a maximum between y = - 150 m and y = -50 m like the simulation based on the reference bathymetry.

For the simulation with the topography with the uniform dune area, the height to which the dune was affected by the erosion, grows from 5.5 m in the south a maximum of 7 m between y = - 150 and y = - 100 and then decreases again southward to 4.5 m at y = 25 m. The slope makes an angle of 45 degrees with the horizontal on average and the dunefoot retreated approximately 6 m, which is equal to the retreat predicted for the reference run. The eroded volume increased southward from around 10 m^3/m to a maximum of 16 m^3/m between y = - 150 m and y = -50 m and then decreases southward again. The eroded volume is about 5 m^3/m higher north of this maximum, between y = - 375 and y = - 200, compared to the prediction for the simulation with the reference bathymetry, but he maximum is comparable to the predictions for the reference simulation.

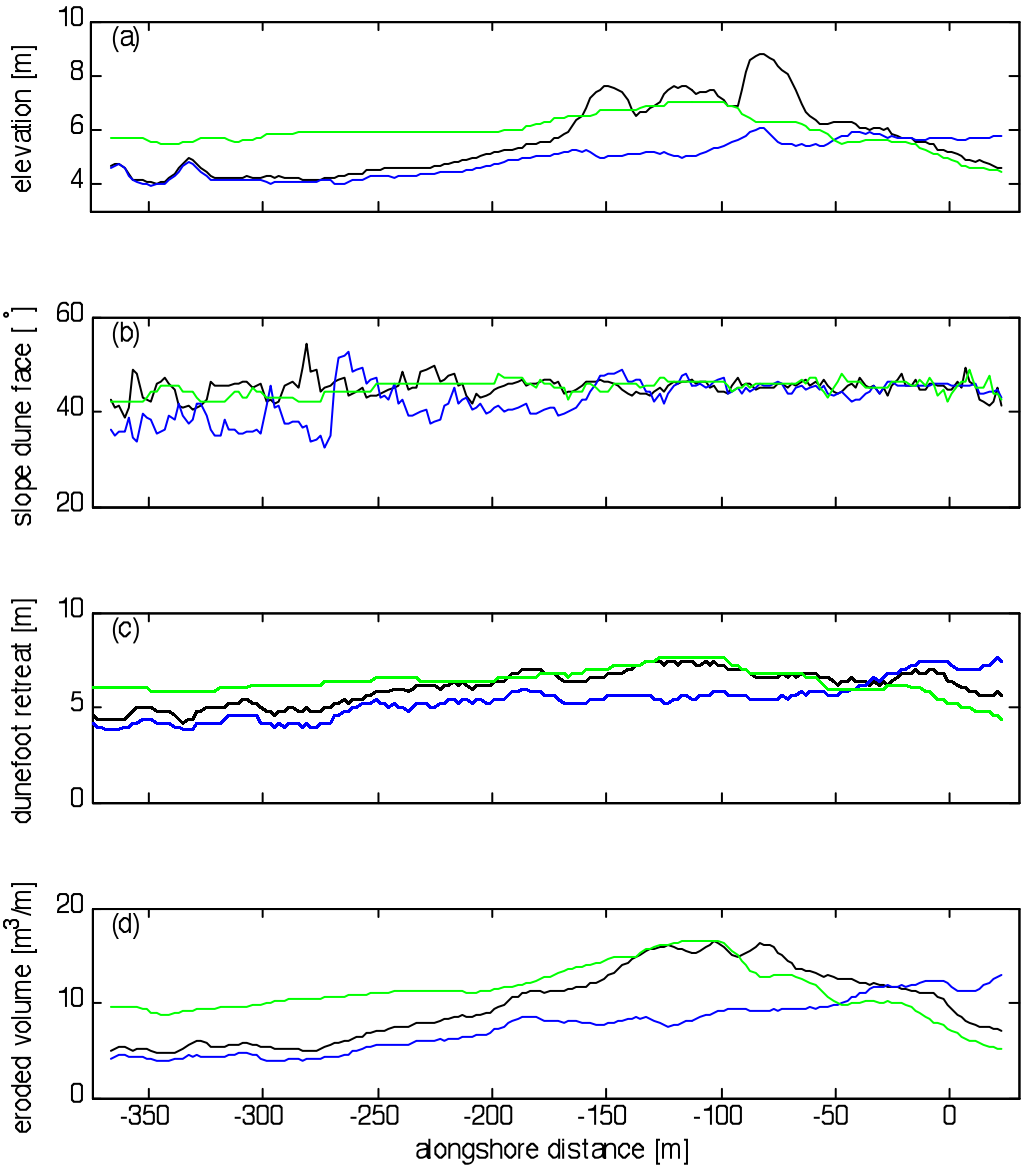

Figure 23 shows the predicted alongshore trends in (a) the height to which the dune face was affected by the dune erosion event (b) the angle of the dune face after the dune erosion event with respect to the horizontal (c) the dunefoot retreat and (d) the eroded volume *V1* between the top of the dune face to the pre-erosion event dune foot, for the measured topography (black), the topography with a uniform bathymetry (blue) and the topography with a uniform dune row (green).

The dune erosion maximum that was predicted for the simulations with the reference topography and the topography with the uniform dune area could be caused by alongshore variations in the bathymetry, and consequently in the on the Hm0,ss and Hm0,inf wave height, because this maximum is not distinct in the dune erosion predicted for the simulation based on the topography with the uniform bathymetry. Therefore we will compare the Hm0,ss and Hm0,inf wave height along 3 cross-

shore transects for the simulation with the initial topography with the uniform bathymetry and the simulation with the observed initial topography.

Figure 24 shows the results for the simulation with the initial topography with the uniform bathymetry. The Hm0,ss wave height, decreases shoreward as the waves break; it was on average 2.8 m along the transect at x = 325.0 m, 1.8 m along the transect at x = 78.1 m and 0.6 m along the transect at x = - 8.9 m. The Hm0,inf wave height was on average 0.3 m along the transect at x = 325.0 m, 0.3 m along the transect at x = 78.1 m and 0.4 m along the transect at x = -8.9 m. The alongshore variation in both the Hm0,ss and the Hm0,inf wave height is neglectable, which could be expected because the initial bathymetry was uniform.

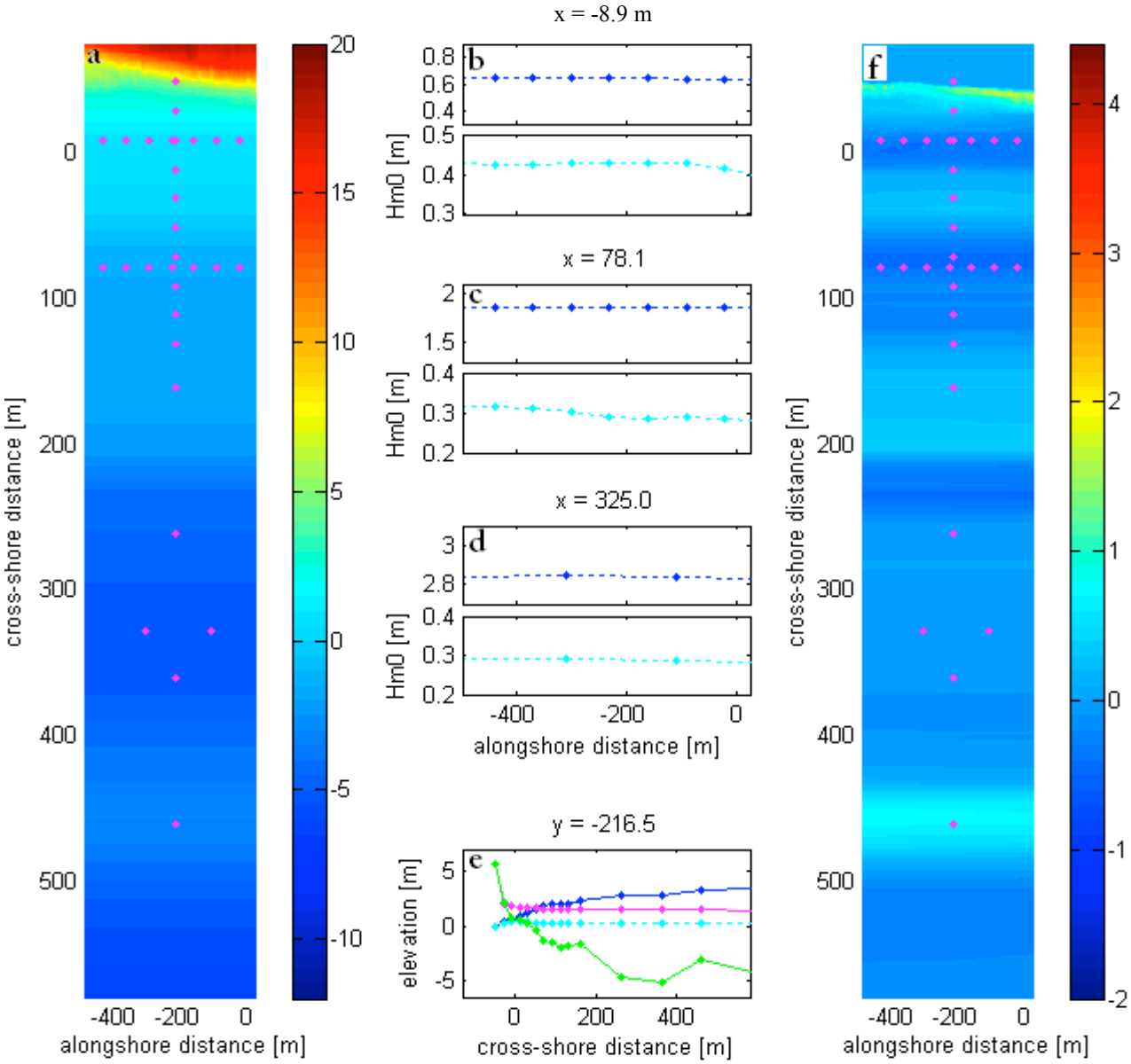

Figure 24 (a) The initial topography with the uniform bathymetry. The pink dots indicate the locations where the Hm0,ss and Hm0,inf were calculated. These were located at three alongshore shore transects at x = -8.9 m, x = 78.1 m and x = 325.0 m and one cross-shore transect at y = - 216.5 m. (b), (c), (d) show the calculated Hm0,ss (blue) and Hm0,inf (cyan) along the alongshore transects and (e) along the cross-shore together with the topography profile (green) and the mean surge level (pink). (f) shows the predicted topographical difference map, also with the output locations.

Figure 25 shows the results for the simulation with the observed initial topography. The Hm0,ss wave height, is around 2.9 m along the transect at x = 325.0 m, 1.7 m to 1.9 m along the transect at x = 78.1 m and 0.6 m to 0.7 m at x = -8.9 m. The location of the maximum in Hm0,ss wave height corresponds to the location of the deeper area in the initial bathymetry and to the dune erosion maximum, but the difference between maximum and minimum Hm0,ss is only 10 cm. The Hm0,inf wave height is on average 0.3 m along the transect at x = 325.0 m, 0.3 m along the transect at x = 78.1 m and ranges between 0.4 m and 0.5 m along the transect at x = -8.9 m.

The Hm0,inf wave height does show a minimum in the location of the dune erosion peak, but this is only 6 cm lower then the max value. So there is some alongshore variation in the Hm0,ss and Hm0,inf wave height due to the alongshore variation in the bathymetry, but 10 cm difference is not enough to explain the alongshore variation in dune erosion. Thus alongshore variation in the bathymetry is not the only cause of alongshore variations in the dune erosion on this scale.

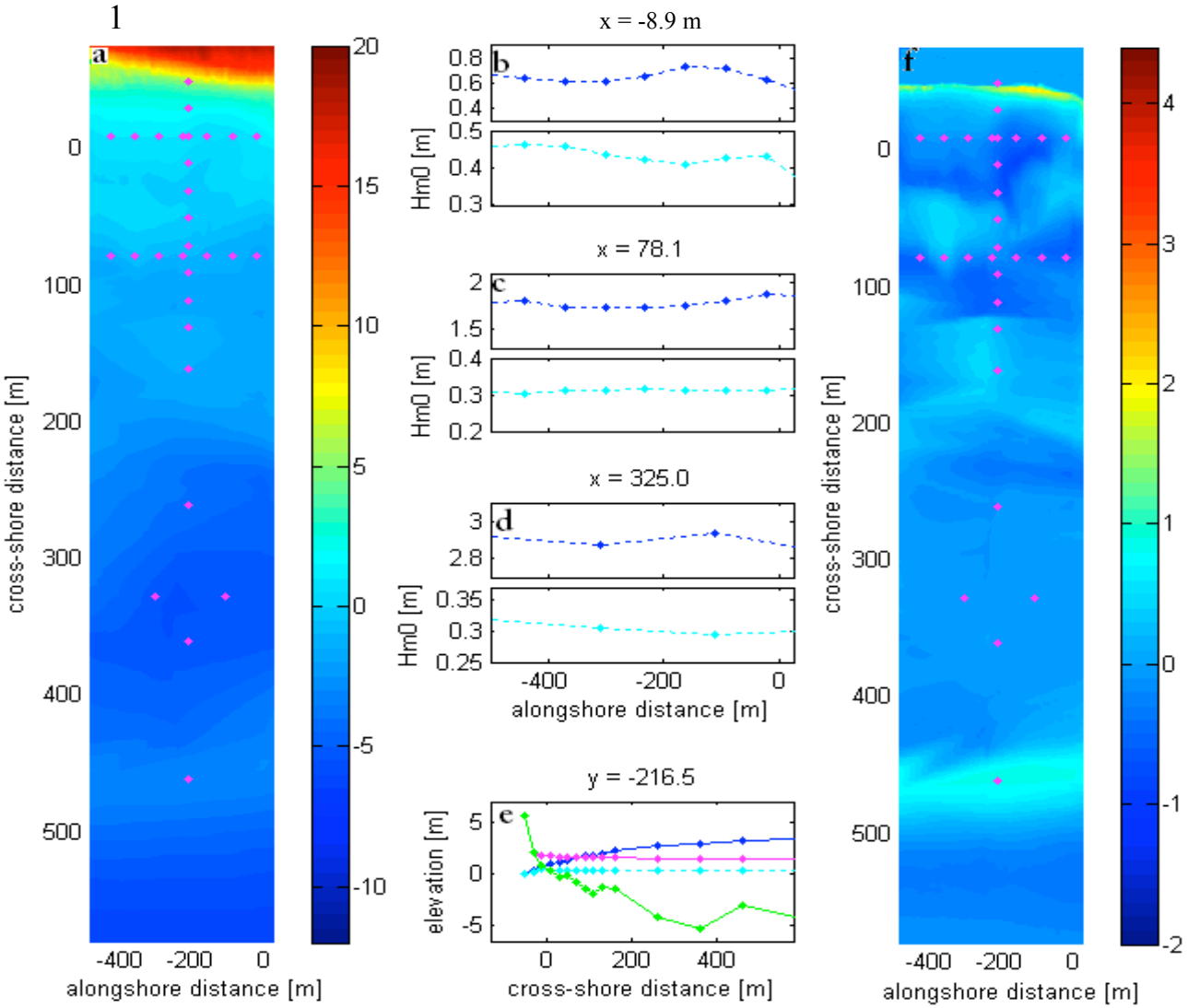

Figure 25 (a) The observed initial topography. The pink dots indicate the locations where the Hm0,ss and Hm0,inf were calculated. These were located at three alongshore shore transects at x = -8.9 m, x = 78.1 m and x = 325.0 m and one cross-shore transect at y = - 216.5 m. (b), (c), (d) show the calculated Hm0,ss (blue) and Hm0,inf (cyan) along the alongshore transects and (e) along the cross-shore together with the topography profile (green) and the mean surge level (pink). (f) shows the predicted topographical difference map, also with the output locations.

5. Discussion

The hydronamic validation results show that XBeach predicts the Hm0,inf wave height reasonably well, but that it overestimates the Hm0,inf wave height, especially when the waves enter the intertidal zone. In section 3.5 it was already suggested that this might be due to uncertainty in the height of the outer bar. One could also try whether using equation 2 of Roelvink(1993) yields better results then using equation 1.

Furthermore, XBeach overestimates dune erosion by approximately 76% when default settings are used for the morphology parameters. However, the default were calibrated by performing laboratory experiments using a depthscale of 1:6. Concequently, the parameter *depthscale,* which scales the morphology parameters eps, hmin, hswitch ans dzmax, should be set to 1/6 for field scale (1:1) simulations. However, 1/6 is to low, because when I only changed the depthscale from 1 to 1/6 in the XBeach model used for the validation, no erosion was predicted anymore. However, this proved that a smaller value for *depthscale* will reduce the overestimation of the eroded volume. This deserves further study.

6. Conclusions

To answer the first main question we compared predictions of the process-based model Xbeach to field observations of the cross-shore wave transformation in the intertidal zone during severe storms. The hydrodynamic calibration showed that the best agreement between the predicted and observed cross-shore wave transformation was found when the free parameters γ and n were set to 0.55 and 10 respectively. For the hydrodynamic validation we performed 8 simulations for different periods with the calibrated hydrodynamic settings. Comparison of the predicted and observed wave height transformation in the intertidal zone for those periods revealed that XBeach predicts the near-shore behaviour of the Hm0,inf wave height reasonably well in 2D mode, with a ε_{rms} of 0.043 and a r^2 of 0.0.29, but that the Hm0,ss wave height is overestimated in 2D mode, with an ε_{rms} of 0.086 and a r^2 of 0.92. We also found that the errors increase, especially for the Hm0,inf wave height prediction, when the simulation is performed in 1D.

To answer the second main question we tested how XBeach simulations compare to field observations of dune erosion and alongshore variation thereof. Comparing the observed to the predicted morphologic response to severe storm conditions showed that the predicted dunefoot retreat was 37% higher than the average observed dunefoot retreat and that the eroded volume is over predicted by 76 % but that the XBeach does reproduce the alongshore trends in the observed dune erosion reasonably well.

To answer the third main question we explored what caused the observed and predicted alongshore variation in dune erosion. Therefore we looked how alongshore variations in the initial bathymetry and the initial dune area influence the predicted dune erosion trends alongshore. We performed three additional simulations with 1. the observed topography, 2. the observed topography with a uniform bathymetry and 3. the observed topography with a uniform dune area.

XBeach predicted the local maximum that was observed in the north of the study area where an embryonic dune field was located, for the simulations with the topographies with the observed dune topography, but not for the simulation with the topography with the uniform dune area. Alongshore variation in the initial dune topography must therefore be the origin of this maximum.

XBeach also predicted the maximum observed in the south of the study area, for the simulations

with the topographies with the observed bathymetry, but not for the simulation with the topography with the uniform bathymetry. This maximum could therefore origin from alongshore variation in the bathymetry or the beach area. To test this we looked at alongshore variations in the Hm0,ss and Hm0,inf wave height caused by alongshore variations in the bathymetry. XBeach predicted 10 cm alongshore variation in the Hm0,ss wave height for the simulation with the observed, non-uniform bathymetry, but this is not enough to explain the strong alongshore variation in dune the erosion, therefore the beach topography must also play a role.

The fact that XBeach predicted alongshore variation in dune erosion for all three initial topographies proves that both alongshore variation in the dune and beach topography and alongshore variation in the bathymetry leads to alongshore variation in the eroded volume.
x = -8.9 m

References

Bolle, A., Mercelis, P. Roelvink, D., Hearens, P. Trouw, K. (2010) Application and validation of Xbeach for three different Field Sites. *Coastal engineering reschearch council.*

Brandenburg, P. (2010) Scale dependency of dune erosion models. MsC Thesis. University of Twente: Holland.

Brinkkemper, J. (2013) Modeling the cross-shore evolution of asymmetry and skewness of surface gravity waves propagating over an intertidal sandbar. MsC Thesis. University Urecht: Holland.

Butt, T., Russell, P. (1999) Suspended sediment transport mechanisms in high energy swash. *Marine geology,* **161**, 261-375

Carter, R.W.G. (1989) Coastal Environments. *Academic Press.* Eigth printing 2002.

Carter, R.W.G. (1991) Near-future sea level impacts on coastal dune landscapes. *Landscape Ecology vol.* 6. 29-39

Carter, R.W.G., Stone, G.W. (1989) Mechanisms associated with the erosion of sand dune cliffs, Magiligan, Northern Ireland. *Earth surface processes and landforms,* **14**, 1-10

Corps of engineers, (1989) Infragravity energy and its implications in nearshore sediment transport and sandbar dynemics. *Department of the Army.*

Claudino‐Sales V., Wang P., Horwitz M.H., (2008) Factors controlling the survival of coastal dunes during multiple hurricane impacts in 2004 and 2005: Santa Rosa barrier island, Florida. *Geomorphology* 95: 295–315

Davindson-Arnott, R. (2010) Introduction to coastal processesn and geomorphology. *Cambridge University Press, New York.*

de Haan, H., Haagsma, I. (1984) Deltawerken: Techniek, politiek en achtergronden. Book, *Waltman; Delft.*

Den Heijer, C., Walstra, D.J.R., van Thiel de Vries, J.S.M, Hoonhout, B.M., Huisman, B.J.A., Diermanse, F.L.M., van Gelder, P.H.A.J.M. (2011) Importance of dune erosion influencing processes. *Journal of Coastal Research*. 283-287

Den Heijer, C., Reniers, A.J.H.M., van de Graaff, J., van Gelder, P.H.A.J.M (2008) Reducing uncertainty in prediction of dune erosion during extreme conditions. ?

Elgar, S., Herbers, T.H.C., Okohiro, M., Oltman-Shay, Guza, R.T. (1992) Observations of Ingragravity Waves. *Journal of geophysical research,* **97**, 15.573-15.577

Galal, E.M., Takawaka, S., (2011) The influence of alongshore and cross-shore wave enery flux on large- and small-scale coastal erosion patterns. *Earth surface processes and landforms* **36** 953-966

Hoonhout, B.M., den Heijer, C. (2010) Reliability of dune erosion assessment along curved coastlines. (?)

Kriebel, D.L., Dean, R.G. (1985) Numerical simulation of time dependent beach and dune erosion. *Coastal Engineering,* **9**, 221-245

Kriebel, D.L., Dean, R.G. (1993) Convolution method for time-dependent beach profile response. *Journal of Waterway, Port, Coastal and Ocean Engineering,* **119 (2)**, 204-226

Masselink, G. Evans, E., Hughes, M.G., Russell, P. 2005. Suspended sediment transport in the swash zone of a dissipative beach. *Marine Geology,* 216, 169-189

McCall, R.T., Van Thiel de Vries, J.S.M. ,Plant, N.G., Van Dongeren, A.R., Roelvink, J.A., Thompson, D.M., Reniers, A.J.H.M. (2010) Two-dimentrional time dependend hurricane overwash and erosion modeling at Santa Rosa Island. *Coastal engineering,* **57,** 668-683

Nishi, R., Kraus, N.C. (1996) Mechanism and calculation of sand dune erosion by storms.

Roelvink, D., Reniers, A., van Dongeren, A., van Thiel de Vries, J., McCall, R., Lescinski, J. (2009) Modelling storm impacts on beaches, dunes and barrier islands. *Coastal engineering,* **56**, 1133-1152

Roelvink, D., Reniers, A., van Dongeren, A., van Thiel de Vries, J., Lescinski, J., McCall, R. (2010) Xbeach Model Describtion and Manual. *Unesco-IHE Institute for Water Education, Deltaris en Delf University of technology.*

Ruessink, B.G., and Jeuken, M.C.J.L., (2002) Dunefoot dynamics along the Dutch coast. *Earth Surface Processes and Landforms*, 27, 1043-1056.

Ruessink, B.G., Boers, M., van Geer, P.F.C., de Bakker, A.T.M., Pieterse, A., Grasso F. and de Winter, R.C., (2012), Towards a process-based model to predict dune erosion along the Dutch Wadden coast. *NederlandsJournan of Geoscience.*

Russel, P.E.., Huntley, D., (1999) A cross-shore sediment transport shape function for high energy beaches. *J. Coastal Res.*

Sallenger A.H., 2000. Storm impact scale for barrier islands. *Journal of Coastal Research* **16**(3) 890–895.

Sheremet, A., Guza, R.t., Elgar, S., Herbers, T.H.C. (2002) Observations of nearshore infragravity waves: Seaward and shoreward propagation components. *Jpurnal og geophysical research,* 107.

Steelzel, H.J. (1993) Cross-shore transport during storm surges. Ph.D Thesis, Delft University of Technology: Holland.

Stockdon H.F., Sallenger A.H., Holman R.A., Howd P.A. 2007. A simple model for the spatially‐variable coastal response to hurricanes. *Marine Geology,* **238**, 1–20

Splinter, K.D., Palmsten, M.L., (2012) Modeling dune response to en East Coast Low. *Marine Geology* 46-57

Technisch Rapport Duinafslag 2006. Beoordeling van de veiligheid van duinen als waterkering ten behoeve and Voorschift Toetsing op Veiligheid 2006. *WL| Delft Hydaulics*

Tucker, M.J, (1954) Surfbeats: sea waves of 1 to 5 minutes' period*. Proc. R. Soc. London*, S**er. A 202**, 565–573.

Van Baak, M.A.X (2002) Storm-erosion effects on safety of sea kikes by probabilistic coastal morphologic modelling. *J.F.K Competition: Coastal, Inland and Ground waters.*

Van de Graaff. J. (2002) Coastal Protection, Structures and (Sea)Dikes. *Coastal Systems and Continental Margins* Volume 6, 229-247

Van Gent, M.R.A., Van Thiel de Vries, J.S.M, Coeveld, E.M., de Vroeg, J.H., van de Van de Graaff, J. (2008). Large-scale dune erosion tests to study the influence of wave periods. *Coastal engenering,* **55**, 1041-1051

Van Rijn, L.C. (2008) Modelling of beach and dune erosion. *Report Z4173/Z4230.* Delft Hydraulics, Delft, The Netherlands

Van Rijn, L.C., Tonnon, P.K., Sanchez-Arcilla, A., Careres, I., Grune, J. (2011) Scaling laws for beach and dune erosion processes. *Caostal engineering,* **58**, 623-636

Thiel de Vries, J., Dongeren, A., McCall, R., & Reniers, A. (2011). The effect of the longshore dimention on dune. Coastal Engineering Proceedings, 1(32), sediment.49.

Van Thiel de Vries, J.S.M, van Gent, M.R.A., Walstra, D.J.R., Reniers, A.J.H.M. (2008). Analysis of dune erosion processes in large-scale flume experiments. *Coastal engenering,* **55**, 1028-1040

Van Tiel de Vries, J. (2009) Dune Erosion During Stoms Surges. Thesis. *Deltaris selected series Vol.* **3.**

Vellinga, P. (1982) Beach and dune erosion during storm surges. *Coastal Engineering,* **6**, 361-387

Vellinga, P. (1986) Beach and Dune Erosion during Storm Surges. Thesis. *Technische universiteit Delft: Holland*

Wetzell L.M, Howd P.A, Sallenger A.H. (2003) Simple models for predicting dune erosion hazards along the Outer Banks of North Carolina. *Proceeding of the International Conference of Coastal Sediments*, 238–422.

Xbeach Manual

Appendix/Appendices

Appendix A Model input file hydrodynamic calibration

General input

depfile = bed.dep
posdwn = 0
nx = 620
ny = 0
alfa = 0
vardx = 1
dy = 10
xfile = x.grd
yfile = y.grd
xori = 0
yori = 0
thetamin = 173
thetamax = 353
dtheta = 10
thetanaut = 1

Initial conditions

zs0 = 1.093846

Model time

tstop = 8200

Physical processes

sedtrans = 0
morphology = 0

Wave boundary condition parameters

instat = 4

Wave breaking parameters

break = 1
gamma = 0.400000
n = 5
breakerdelay = 0

Wave-spectrum boundary condition parameters

bcfile = waves.txt
rt = 8200
dtbc = 1

Appendix B1 Model input file hydrodynamic validation

Flow boundary condition parameters

epsi = -1

Grid parameters

depfile = bed.dep
posdwn = 0
nx = 433
ny = 126
alfa = 0
vardx = 1
dy = 5
xfile = x.grd
yfile = y.grd
xori = 0
yori = 0
thetamin = -90
thetamax = 90
dtheta = 10
thetanaut = 0

Initial conditions

zs0 = 1.133385

Model time

tstop = 8200

Physical processes

sedtrans = 0
morphology = 0

Sediment transport parameters

swtable = swtable.txt

Wave boundary condition parameters

instat = jons

Wave breaking parameters

break = 1
gamma = 0.550000
n = 10
breakerdelay = 0

Wave-spectrum boundary condition parameters

bcfile = jonswap

rt = 8200
dtbc = 1

Appendix B2 Model input file morphodynamic validation

Flow boundary condition parameters
epsi = -1
Grid parameters
posdwn = 0
nx = 489
ny = 72
alfa = 0
vardx = 1
dy = 5
xfile = x.grd
yfile = y.grd
xori = -314
yori = -74.000000
thetamin = -90
thetamax = 90
dtheta = 10
thetanaut = 0
Model time
tstop = 369000
Morphology parameters
morfac = 5
Physical processes
sedtrans = 1
morphology = 1
Sediment transport parameters
swtable = swtable.txt
Tide boundary conditions
zs0file = tide.txt
tideloc = 1
Wave boundary condition parameters
instat = 41
Wave breaking parameters
break = 1
gamma = 0.550000

n = 10

breakerdelay = 0

Wave-spectrum boundary condition parameters

bcfile = waves.txt

rt = 369000

dtbc = 1